The global geometry of phase-resetting surfaces: the role of critical level sets and isochrons

Peter Langfield

Inria Bordeaux – Sud-Ouest, Talence, France and IHU Liryc, Fondation Bordeaux Université, Pessac-Bordeaux, France

Bernd Krauskopf Kyoung Hyun Lee Hinke M. Osinga

Department of Mathematics and Dodd–Walls Centre for Photonic and Quantum Technologies, University of Auckland, Private Bag 92019, Auckland 1142, New Zealand

February 2025

Abstract

Given a system with a stable oscillation represented by an underlying attracting periodic orbit Γ, what is its reaction to perturbations in a fixed direction $\mathbf{d}$ for any amplitude A of the perturbation? Such phase resets are often expressed by the phase transition curve (PTC) that, for fixed $A \geq 0$, relates the 'old' or 'original' phase ϑ_{o} in the cycle, at which the perturbation is applied, to the 'new' phase ϑ_{n} one observes after relaxation back to the stable oscillation. It is well known that the nature of the PTC changes with A, and this can be represented by the *phase-resetting surface*, defined as the graph of the function $\mathcal{P}_{\mathbf{d}}(\vartheta_{\mathrm{o}}, A)$ that assigns ϑ_{n} to every combination of $(\vartheta_{\mathrm{o}}, A)$-pairs for which the associated phase reset in the direction $\mathbf{d}$ returns to Γ.

We study the phase-resetting surface $\mathrm{graph}(\mathcal{P}_{\mathbf{d}}(\vartheta_{\mathrm{o}}, A))$ by considering the properties of its level sets. This work is motivated by sketches from the 1970s of such level sets for the four-dimensional Hodgkin–Huxley model; Eric Best drew these sketches by hand, after performing numerical integrations over a grid of perturbations in the $(\vartheta_{\mathrm{o}}, A)$-plane. Best accurately captured the general arrangement of level sets, but was not able to resolve them in certain regions. By making use of a numerical setup based on the formulation of suitable boundary value problems, we are able to complete Best's sketch via the computation of many level sets of the phase-resetting surface directly as curves in the $(\vartheta_{\mathrm{o}}, A)$-plane.

The theoretical underpinning for this approach is the realization that the level sets are the intersection sets of a half-cylinder, comprising translations of Γ in the direction $\mathbf{d}$, with the isochrons of Γ. The isochrons are submanifolds of codimension one consisting of all points that approach Γ with a given phase, and they foliate the basin of attraction of Γ. With our geometric approach, we identify critical level sets and associated isochrons characterized by certain tangencies with the two-dimensional half-cylinder. We illustrate with two examples of planar vector fields that critical level sets are generally a geometric necessity and, hence, do not merely arise because the Hodgkin–Huxley model is of higher dimension.

The work presented here also demonstrates, from a more general perspective, that computing (level sets of) $\mathrm{graph}(\mathcal{P}_{\mathbf{d}}(\vartheta_{\mathrm{o}}, A))$ for one or several suitable directions $\mathbf{d}$ is an effective way to investigate foliations of basins of attraction by isochrons of dimensions two or higher.

1 Introduction

Determining the response of an oscillating cell to a given stimulus applied at different times in the cycle is a well-known technique to gain insights into internal cellular properties or mechanisms. When the system returns to stable oscillations, it does so generally with a phase shift compared to the unperturbed oscillations. Recording this phase shift as a function of the (old or original) phase ϑ_{o} in the cycle at which the perturbation is applied, gives the *phase response curve* (PRC). Alternatively and equivalently, one can consider the *phase transition curve* (PTC), which records the resulting (new) phase ϑ_{n}, rather than the phase shift $\vartheta_{\mathrm{n}}-\vartheta_{\mathrm{o}}$, as a function of ϑ_{o}. Both the PRC and the PTC have been used to distinguish different types of oscillating cells, including neurons and cardiac cells; for example, see [3, 10, 11, 12, 18, 19].

From the mathematical perspective, it is more straightforward to consider the PTC; here both ϑ_{o} and ϑ_{n} represent fractions of the underlying period, that is, they lie in the interval $[0,1)$. This point of view has been taken and popularized by the pioneering theoretical biologist Arthur Winfree [14, 34, 36], who studied how the PTC changes as the amplitude of a specific perturbation is varied. For low amplitudes, the phase ϑ_{n} increases or decreases by 1 when ϑ_{o} increases from 0 to 1, which is known as type-1 or weak phase resetting. For larger amplitudes, however, one typically finds that ϑ_{n} neither increases nor decreases on average; this is called type-0 or strong phase resetting. Winfree observed these two types of phase resetting, as well as the transition between them, in extensive experiments [34] with the yeast cycle and with hatching fruit flies, where he changed both the phase ϑ_{o} of the perturbation and its amplitude, which we refer to as A. Winfree obtained hundreds of data points giving the resulting values of ϑ_{n} over a large region of the $(\vartheta_{\mathrm{o}}, A)$-plane. He identified a point of phase singularity as being responsible for the transition of the PTCs from type 1 to type 0. Moreover, he represented the recorded phase responses as a surface in $(\vartheta_{\mathrm{o}}, A, \vartheta_{\mathrm{n}})$-space, which he determined to be a helicoid with a vertical "singular axis" at the phase singularity.

Winfree was well aware that the point of phase singularity corresponds to a special reset that perturbs a specific point in the cycle to a point in the boundary of the basin of attraction. All points in the basin, on the other hand, return to the oscillation in sync with a point of a particular phase. Winfree defined an isochron as all points in the basin with the same "latent phase" [36]. In this more theoretical context, one assumes that the system under investigation is described by a mathematical model in the form of an m-dimensional autonomous vector field

$$\dot{\mathbf{x}} = \mathbf{F}(\mathbf{x}), \tag{1}$$

where $\mathbf{F} : \mathbb{R}^m \to \mathbb{R}^m$ is sufficiently smooth. The oscillation under consideration is then given as a stable periodic orbit Γ with (minimal) period T_Γ, which is parameterized as $\Gamma = \{\gamma_\vartheta = \Phi(\vartheta T_\Gamma, \gamma_0) \mid \vartheta \in [0,1)\}$ by the phase variable $\vartheta \in \mathbb{S}^1$, represented by the interval $[0,1)$; here, $\Phi(t,\cdot)$ is the flow of (1) and γ_0 is a reference point on Γ. As is the convention, we choose the zero-phase point γ_0 as the point on Γ with the maximal value of the first component of the vector $\mathbf{x} \in \mathbb{R}^m$. Guckenheimer [15] showed that the isochrons I_ϑ for $\vartheta \in [0,1)$ form a one-parameter family of smooth $(m-1)$-dimensional manifolds that are transverse to Γ and foliate its basin of attraction $\mathcal{B}(\Gamma)$. Therefore, the question of finding the phase response of resets in some direction $\mathbf{d} \subset \mathbb{R}^m$ with amplitude $A \geq 0$ boils down to checking which isochrons are 'hit' when the points on Γ are perturbed. We assume that these perturbations are instantaneous, that is, they can be expressed via the perturbation map

$$\begin{array}{rccc} \Upsilon_{\mathbf{d}} & : & \mathbb{S}^1 \times \mathbb{R}_0^+ & \to & \mathbb{R}^m \\ & & (\vartheta_{\mathrm{o}}, \quad A) & \mapsto & \gamma_{\vartheta_{\mathrm{o}}} + A\,\mathbf{d}, \end{array} \tag{2}$$

where the unit vector $\mathbf{d} \in \mathbb{S}^{m-1} \subset \mathbb{R}^m$ is fixed.

This geometric point of view motivates us to consider the general phase-resetting map

$$\begin{array}{rcccc} \mathcal{P} & : & \mathbb{S}^1 \times \mathbb{S}^{m-1} \times \mathbb{R}_0^+ & \to & \mathbb{S}^1 \\ & & (\vartheta_\mathrm{o}, \quad \mathbf{d}, \quad A) & \mapsto & \vartheta_\mathrm{n}, \end{array} \tag{3}$$

which is defined by the property that

$$\Upsilon_{\mathbf{d}}(\vartheta_\mathrm{o}, A) = \gamma_{\vartheta_\mathrm{o}} + A\,\mathbf{d} \in I_{\vartheta_\mathrm{n}}, \tag{4}$$

provided this phase reset from the point $\gamma_{\vartheta_\mathrm{o}} \in \Gamma$ lies in $\mathcal{B}(\Gamma)$; otherwise, $\mathcal{P}(\vartheta_\mathrm{o}, \varphi_\mathrm{d}, A)$ is undefined. In previous work [27] we considered the function $\mathcal{P}$ for planar systems as a function of all inputs; in particular, we allowed the direction vector $\mathbf{d}$ to vary, which in the planar case can be defined by a second periodic variable $\varphi_\mathrm{d} \in \mathbb{S}^1$. More specifically, we considered the concept of directional transition curves (DTCs) and associated phase-resetting surfaces $\mathrm{graph}(\mathcal{P}_A)$ with $\mathcal{P}_A(\vartheta_\mathrm{o}, \varphi_\mathrm{d}) := \mathcal{P}(\vartheta_\mathrm{o}, \varphi_\mathrm{d}, A)$ for fixed amplitude A.

In this paper, we take the 'more traditional' point of view already adopted by Winfree and consider the case that the direction $\mathbf{d}$ of the perturbations remains fixed. In other words, we study the function $\mathcal{P}_\mathbf{d}(\vartheta_\mathrm{o}, A) := \mathcal{P}(\vartheta, \mathbf{d}, A)$ and the geometric properties of the corresponding phase-resetting surface $\mathrm{graph}(\mathcal{P}_\mathbf{d})$. The new aspect is that we investigate the phase-resetting map $\mathcal{P}_\mathbf{d}$ for the case that the underlying model has a phase space of dimension larger than two. Phase resetting for an m-dimensional system with $m \geq 3$ in a specific direction $\mathbf{d}$ can be understood geometrically as the question of how the $(m-1)$-dimensional isochrons of the given attracting periodic orbit Γ are intersected by the *attainable half-cylinder*

$$\mathcal{C}_\mathbf{d} := \mathrm{range}(\Upsilon_\mathbf{d}) = \{\gamma + A\,\mathbf{d} \in \mathbb{R}^m \mid \gamma \in \Gamma \text{ and } A \in \mathbb{R}_0^+\}, \tag{5}$$

consisting of all non-negative translations of Γ along the vector $\mathbf{d}$. Note that $\mathcal{C}_\mathbf{d}$ is parameterized by phase $\vartheta_\mathrm{o} \in [0, 1)$ and amplitude A, with Γ given by $A = 0$. Hence, the $(\vartheta_\mathrm{o}, A)$-plane, which is the covering space of $\mathbb{S}^1 \times \mathbb{R}_0^+$, is a natural 'flat' representation of $\mathcal{C}_\mathbf{d}$.

In the late 1970s, Arthur Winfree [34, 36, 37] already understood that the resulting intersection sets of the isochrons are typically one-dimensional curves. His PhD student Eric Best [2] computed them numerically for the four-dimensional Hodgkin–Huxley model [20] to check the validity of the model in terms of how the phase-resetting pattern matches that found in experiments; the details of the Hodgkin–Huxley model as used by Best are given in Section 3. Figure 1 is a reproduction of Best's image of level sets from [2, Figure 11]; see also [37, pp 154–155] for alternative depictions of this figure by Winfree, and [4, 33] for other examples. In Fig. 1, the phase (ϑ_o in our notation) runs horizontally from 0 to 1, and the amplitude (A in our notation) is shown along the vertical axis over the range $[-60, 60]$. The latter suggests that Best considered $A \in \mathbb{R}$ of any sign, which means that he effectively 'glued' the two half-cylinders $\mathcal{C}_\mathbf{d}$ and $\mathcal{C}_{-\mathbf{d}}$ along Γ, to obtain a full cylinder extending in both directions $\mathbf{d}$ and $-\mathbf{d}$. As Fig. 1 shows, Best computed the asymptotic phases ϑ_n by numerical simulation for a grid of 20 by 16 points in the shown region of the $(\vartheta_\mathrm{o}, A)$-plane; here, each grid point defines a reset at phase ϑ_o in the cycle that instantaneously shifts the membrane voltage of the Hodgkin–Huxley model by the value A. Best calculated the resulting asymptotic phase ϑ_n in terms of a percentage of one complete cycle by integrating the perturbed point over several multiples of the period of Γ, until it reached sufficient proximity to one of one-hundred uniformly-distributed phase points on Γ. The main goal in [2] was to identify stimuli applied during the action potential that resulted in a sudden termination of the firing action — called "oscillator death" by Winfree [34]. Mathematically, such $(\vartheta_\mathrm{o}, A)$-pairs lead to resets outside the basin of attraction of Γ. Best calls the corresponding regions the "null space" of Γ, and they are shaded with a horizontal-hatch pattern in Fig. 1.

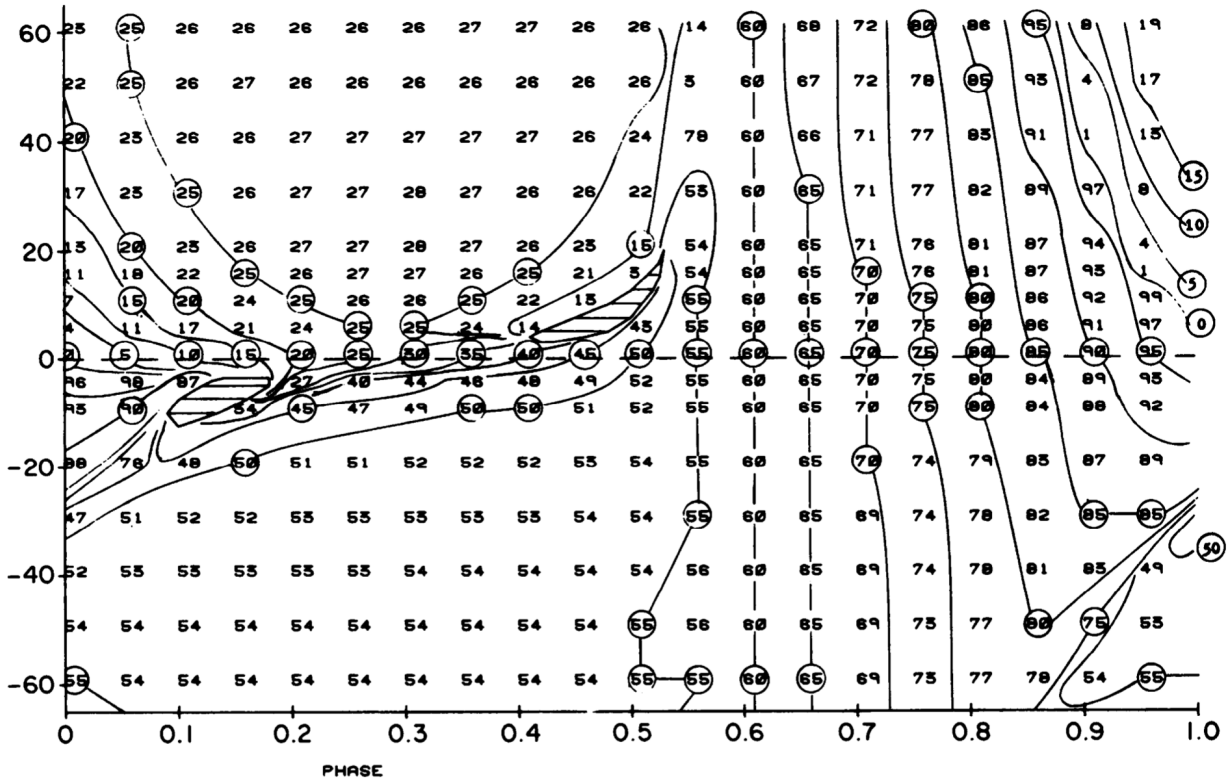

Figure 1: Level sets of the phase-resetting surface for the Hodgkin–Huxley model (8) in the direction $\mathbf{d} = (1, 0, 0, 0)^{\mathrm{T}}$, as drawn by Best based on computations of latent phase over the shown grid in the phase-amplitude plane. Reprinted from Biophysical Journal, 27(1), E.N. Best, Null space in the HodgkinHuxley equations, 87-104, Copyright (1979), with permission from Elsevier.

The data points in Fig. 1 provide some indication of the level sets of equal asymptotic phase in the $(\vartheta_{\mathrm{o}}, A)$-plane, which Best attempted to draw by hand for 20 phases at 5% intervals along the cycle. Figure 1 shows that the structure of the level sets is quite complicated and difficult to resolve overall with the method employed by Best. A few features stand out, and we first discuss those for phase resets with positive amplitudes. Best's level sets 60 to 95 leave the shown range at the top for increasing A and do not seem to return. Level sets 30 to 55, on the other hand, are shown to approach the region of oscillator death for $A \geq 0$ in a seemingly spiraling fashion. A special case is level set 25, which appears to consist of two segments: a first segment leaving at the top to the left, and a second coming from the top, passing very close to the first segment, and then also converging to the region of oscillator death. Level set 15 is also sketched as 'reappearing from the top' in this way; similarly, while they are not shown to reappear explicitly, Fig. 1 suggests that level sets 0 to 10 and 20 behave in the same way. Noticeable is also the large region above level set 25, where ϑ_{n} hardly changes and percentage values are either 26 or 27 throughout. The structure of the sketched level sets for $A \leq 0$ in Fig. 1 is somewhat similar. Those for 5 to 50 and 80 to 95 appear to approach the region of oscillator death for negative perturbations directly, while those for 55 to 75 appear to leave the shown range at the bottom and then 'reappear' to approach the region of oscillator death. For $A \leq 0$, there is also a large region where the new phase only varies between 52 and 54.

In this paper we employ a numerical method that allows us to compute level sets of the phase-resetting surface $\mathrm{graph}(\mathcal{P}_{\mathbf{d}}(\vartheta_{\mathrm{o}}, A))$ directly; this is achieved via the continuation of solution families of a multi-segment boundary value problem. Specifically, this geometric approach allows

us to complete Best's sketch in Fig. 1 for the four-dimensional Hodgkin–Huxley model in the sense that we are able to explain the geometry of all level sets in the (ϑ_o, A)-plane. First of all, we show that not some, but all level sets spiral around and approach the two regions of oscillator death by performing very sharp or hooked turns, also called "boomerang turns", which are a known feature of one-dimensional isochrons of planar systems with a time-scale splitting [23, 24, 30]. Secondly, we show that there exist special level sets, which we call *critical level sets*, characterized by tangencies between the cylinder $\mathcal{C}_\mathbf{d}$ and a corresponding critical isochron. We identify two kinds of critical level sets: those due to tangencies for finite A and those due to tangencies in the limit of infinitely large A. As we show with two examples of planar vector fields, critical level sets are a geometric necessity when isochrons accumulate on a closed curve or singular point in the (ϑ_o, A)-plane at which the new phase ϑ_n is not defined.

From a more general perspective, the work presented here also demonstrates that it is possible to determine reliably the geometric structure of their one-dimensional intersection sets, regardless of the dimension of the isochrons. Note that it is already challenging to compute two-dimensional isochrons in mathematical models of dimension $m = 3$; see [28, 31] for recent examples. In phase spaces of dimension $m \geq 4$, as is the case for the Hodgkin–Huxley model considered here, there is also the additional challenge of visualizing the $(m-1)$-dimensional isochrons. However, we show that the geometry of the isochrons and the basin itself can reliably be probed in the more restricted context of phase resetting, where only perturbations in certain directions are practical or relevant. Geometrically, the cylinder $\mathcal{C}_\mathbf{d}$ 'drills through' phase space much like when coring an apple or, better, a cabbage: the resulting isochron 'slices' in the (ϑ_o, A)-plane are exactly the levels sets of $\mathrm{graph}(\mathcal{P}_\mathbf{d})$ in terms of the corresponding new phase ϑ_n when plotted in $(\vartheta_o, A, \vartheta_n)$-space. In particular, it is not necessary to compute the isochrons themselves as hypersurfaces to determine their relevant slices.

The paper is organized as follows. In Section 2 we introduce level sets formally and present their relevant properties. In Section 3, we introduce the Hodgkin–Huxley model, present our version of Best's image in Section 3.1, and discuss the nature of the accumulation on the singular set in Section 3.2. To aid the subsequent discussion, we then discuss two planar examples in Section 4: Winfree's model with a 'hole' in Section 4.1, and the FitzHugh–Nagumo system in Section 4.2. The overall level-set geometry of the Hodgkin–Huxley model is the subject of Section 5. Specifically, we show in Sections 5.1 how a critical level set bounds an isola of concentric level curves, while Section 5.2 discusses the critical level set that extends to infinity. In Section 6, we draw some conclusion and present an outlook to future work. A details our computational approach to computing level curves of the phase-resetting surface.

2 General properties of level sets

It is convenient to consider a selection of level sets of the phase-resetting surface $\mathrm{graph}(\mathcal{P}_\mathbf{d}(\vartheta_o, A))$ in projection onto the (ϑ_o, A)-plane, where they are height lines of the 'topographic map' representing the surface. Indeed, the 20 curves in Fig. 1 by Best are an example of representing the phase response this way, as is Winfree's version of this figure on page 155 in [37]. Additionally, the value of ϑ_n can be represented by color for the selected level sets, or even for every point of the (ϑ_o, A)-plane; see, for example, the figure in [37, page 154], or [4, Fig. 8] and [33, Fig. 5]. We now discuss some relevant general properties of these level sets, which we refer to as L_ϑ from now on. As was mentioned in the introduction, a level set L_ϑ is defined as

$$L_\vartheta := \{(\vartheta_o, A) \in \mathbb{S}^1 \times \mathbb{R}_0^+ \mid \mathcal{P}_\mathbf{d}(\vartheta_o, A) = \vartheta\}.$$

Equivalently, L_ϑ can be defined in terms of the perturbation map $\Upsilon_{\mathbf{d}}$ from definition (2), as

$$L_\vartheta := \Upsilon_{\mathbf{d}}^{-1}(I_\vartheta) = \Upsilon_{\mathbf{d}}^{-1}(I_\vartheta \cap \mathcal{C}_{\mathbf{d}}) = \{(\vartheta_\mathrm{o}, A) \in \mathbb{S}^1 \times \mathbb{R}_0^+ \mid \Upsilon_{\mathbf{d}}(\vartheta_\mathrm{o}, A) \in I_\vartheta\}. \tag{6}$$

This formulation is especially convenient when one considers the much-studied special case $m = 2$ of a planar system [27].

It follows from either of these characterizations that each level set L_ϑ is generically a set of smooth curves. More specifically, all level sets L_ϑ are transverse to the line with $A = 0$; this follows from the fact that the $(m-1)$-dimensional isochron I_ϑ is the stable manifold of the attracting (hyperbolic) fixed point γ_ϑ of the time-T_Γ map. In particular, I_ϑ is tangent to the stable eigenspace of the time-T_Γ map and, hence, transverse to Γ; see also [15]. Therefore, the point $(\vartheta_\mathrm{o}, 0)$ can be continued locally as a smooth level curve when A is increased from $A = 0$; we call it the *primary level curve* in L_ϑ. Hence, L_ϑ is never empty. From the computational perspective, the primary level curve in L_ϑ can readily be computed by continuation from the corresponding phase point on the line $\{A = 0\}$ as a curve parameterized by arclength. Should they exist, other level curves in L_ϑ must be started by performing one or more intermediate homotopy steps; see A for further explanation of our computational setup.

An important element of phase resetting are points or open regions in the $(\vartheta_\mathrm{o}, A)$-plane where the new phase ϑ_n is not defined. The "null spaces of oscillator death" in Fig. 1 are a specific example. We prefer to talk about the *singular set* S, defined as

$$S := \{(\vartheta_\mathrm{o}, A) \in \mathbb{S}^1 \times \mathbb{R}_0^+ \mid \Upsilon_{\mathbf{d}}(\vartheta_\mathrm{o}, A) \notin \mathcal{B}(\Gamma)\} = \Upsilon_{\mathbf{d}}^{-1}(\mathbb{R}^m \setminus \mathcal{B}(\Gamma)) = \mathbb{R}^m \setminus \mathcal{B}(\Gamma) \cap \mathcal{C}_{\mathbf{d}}, \tag{7}$$

where $\mathbb{R}^m \setminus \mathcal{B}(\Gamma)$ is the complement of the basin $\mathcal{B}(\Gamma)$ in $\mathbb{R}^m$. Clearly S depends on $\mathbf{d}$, but we do not explicitly indicate this dependence for notational convenience. The boundary $\partial\mathcal{B}(\Gamma)$ of the basin $\mathcal{B}(\Gamma)$, which is also the boundary of its complement, can be very complicated in $\mathbb{R}^m$ if $m \geq 3$. In particular, it may contain compact saddle invariant objects and their stable manifolds of different dimensions. General theory of intersecting manifolds [1, 7, 32] states that the boundary ∂S of the singular set, which is the intersection set of $\partial\mathcal{B}(\Gamma)$ and the two-dimensional cylinder $\mathcal{C}_{\mathbf{d}}$, will typically be a set comprising isolated points (generic intersections with $(m-2)$-dimensional invariant, stable manifolds) and/or smooth curves (generic intersections with $(m-1)$-dimensional invariant, stable manifolds). Intersections with lower-dimensional invariant objects, on the other hand, are exceptional because they are destroyed by small perturbations (of the direction $\mathbf{d}$, for example, or of system parameters).

The structure of S may be very complicated when $\partial\mathcal{B}(\Gamma)$ is complicated and is intersected by $\mathcal{C}_{\mathbf{d}}$ in many different components. However, the 'classical case' that we already know from planar systems is that S consists of a single point or of a closed topological disk (simply connected region). The latter is the case of "null spaces of oscillator death" that Best and Winfree encountered in their study of the four-dimensional Hodgkin–Huxley model. Best and Winfree found two such disks in Fig. 1, one for positive and one for negative A, that is, a single disk in each of their half-cylinders $\mathcal{C}_{\mathbf{d}}$ and $\mathcal{C}_{-\mathbf{d}}$.

The 'topological puzzle' inherent in Fig. 1 is how the level sets foliate the complement of the singular set S in the $(\vartheta_\mathrm{o}, A)$-plane for $A \geq 0$, as well as the complement of S_- for $A \leq 0$. The first question in this context is where each of the primary level curves ends up. Importantly, general theory states that all isochrons I_ϑ accumulate on $\partial\mathcal{B}(\Gamma)$ [15, 35], which is also known as the phaseless set [35, 36]. This fact implies, in turn, that all level sets L_ϑ accumulate on the boundary ∂S of the singular set. The second question is, therefore, how this occurs, because the accumulating curve need not be the primary level curve. And finally, the question arises whether there are any level sets L_ϑ that have more than one connected component. We proceed by showing that these

C_m	=	1.0	(μF cm^{-2}),	I_{app}	=	-8.75	(A cm^{-2}),
V_{Na}	=	-115	(mV),	g_{Na}	=	120	(mS cm^{-2}),
V_K	=	12	(mV),	g_K	=	36	(mS cm^{-2}),
V_L	=	-10.59892097	(mV),	g_L	=	0.3	(mS cm^{-2}).

Table 1: Values taken from [2] for the parameters used in the Hodgkin–Huxley model (8).

three question can be addressed effectively with our computational approach of computing level curves directly.

3 Level sets of the phase-resetting surface of the Hodgkin–Huxley model

The four-dimensional Hodgkin–Huxley model [20] describes mathematically the generation and propagation of action potentials that Hodgkin and Huxley measured experimentally in a space-clamped squid axon. We use, and repeat here for convenience, the system of four ordinary differential equations as given by Best [2]:

$$\begin{cases} C_m \dot{V} &= I_{app} - \left[g_K\,(V-V_K)n^4 + g_{NA}h(V-V_{Na})m^3 + g_L(V-V_L)\right], \\ \dot{m} &= \alpha_m(V)\,(1-m) - \beta_m(V)\,m, \\ \dot{n} &= \alpha_n(V)\,(1-n) - \beta_n(V)\,n, \\ \dot{h} &= \alpha_h(V)\,(1-h) - \beta_h(V)\,h. \end{cases} \tag{8}$$

They model the voltage potential V across the cell membrane, mediated by sodium, potassium, and a leak current; the dynamics for the sodium and potassion ion channels are described by gating variables denoted m, n, and h. The voltage-dependent transition rates α_x and β_x, for $x \in \{m,\, n,\, h\}$, are defined as

$$\begin{aligned} \alpha_m(V) &= 0.1\,(V+25.0)\left[e^{(V+25.0)/10.0}-1.0\right]^{-1}, & \beta_m(V) &= 4.0\,e^{V/18.0}, \\ \alpha_n(V) &= 0.01\,(V+10.0)\left[e^{(V+10.0)/10.0}-1.0\right]^{-1}, & \beta_n(V) &= 0.125\,e^{V/80.0}, \\ \alpha_h(V) &= 0.07\,e^{V/20.0}, & \beta_h(V) &= \left[e^{(V+30.0)/10.0}+1.0\right]^{-1}. \end{aligned} \tag{9}$$

Note here the scale factor of 0.01 in the equation for α_n in accordance with the form given in [20], which appears incorrectly in [2].

A constant current I_{app} must be applied to elicit a spontaneous rhythmically-firing action potential, corresponding to the existence of an attracting periodic orbit Γ; we use the parameters given in Table 1, as chosen by Best [2], for which Γ has period $T_\Gamma \approx 15.4128$ and there also exists a stable equilibrium at $(V, m, n, h) \approx (-4.9492,\, 0.0931,\, 0.3955,\, 0.4199)$.

3.1 The level sets of Best computed as smooth curves

Figure 2 shows (approximately) the same 20 level sets computed by Best in Fig. 1, which we computed with our continuation method (see A) as the primary level curves starting from appropriate points on the horizontal line $\{A = 0\}$. To aid comparison, they are shown over the same range of the $(\vartheta_{\text{o}}, A)$-plane; the light-gray shaded regions in Fig. 2 are the two singular disks that correspond

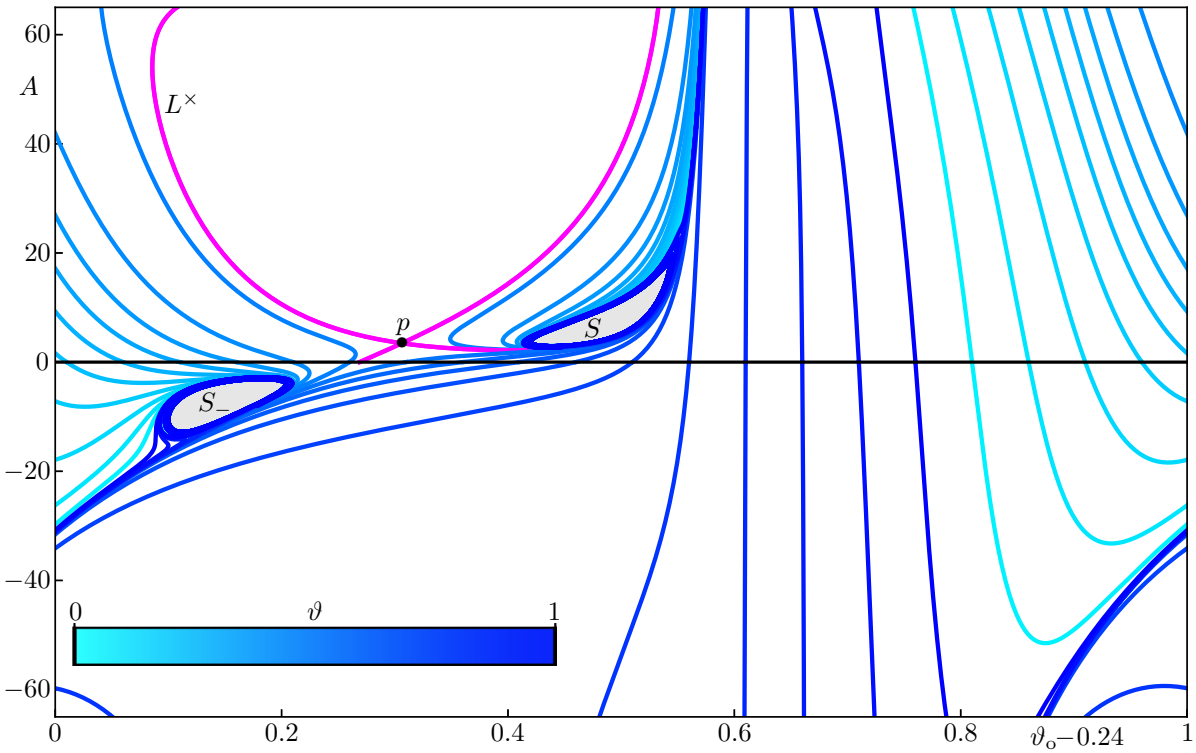

Figure 2: Computed primary level curves in the (ϑ_o, A)-plane of graph$(\mathcal{P}_\mathbf{d})$ for the Hodgkin–Huxley model (8) in the direction $\mathbf{d} = (1, 0, 0, 0)^T$, for both $A \geq 0$ and $A \leq 0$. Shown are 20 level sets L_ϑ that are colored in shades from cyan to dark blue according to the value of ϑ as indicated by the color bar. These level sets are uniform in ϑ and chosen to represent approximately those sketched by Best in Fig. 1; and the ϑ_o-axis is shifted to agree with his choice of the zero-phase point. The light-gray shaded regions are the singular sets S and S_- of oscillator death. Additionally we show the critical level set $L^\times$ (magenta) characterized by containing a critical point p.

to the hatched regions in Fig. 1. As is the convention, we define the point $\gamma_0 \in \Gamma$ with zero phase as having the maximum value of the first variable V. However, Best chose a different starting point for his phase computation, which he reports as $(V, m, n, h) = (4.82, 0.030, 0.450, 0.397)$; we determined that this point is an approximation of the point $\gamma_\vartheta \in \Gamma$ with phase $\vartheta \approx 0.2364 \approx 0.24$, according to the standard convention. For ease of comparison with Fig. 1, the 20 level curves in Fig. 2 are those in L_ϑ with $\vartheta = 0.04 + k\,0.05$, for $k = 0, 1, \ldots, 19$. Throughout, we show any computed level sets of the Hodgkin–Huxley model (8) with a ϑ_o-axis that is shifted by 0.24, so that the shown range $[0, 1]$ agrees with that of Best. The level sets are colored in shades from cyan to dark blue according to their phases ϑ (with respect to γ_0) as indicated by the color bar.

Comparing Figs. 1 and 2, we see that the general structure of the selected primary level curves agree. An advantage of our approach is that we compute the primary level curves directly as arclength-parameterized curves, which enables us to resolve more detail. First of all, in agreement with the image of Best, the curves, indeed, leave Fig. 2 at the top and bottom, respectively, and then return to the shown range of A. Our computations show that all these primary level curves accumulate on S for $A \geq 0$ and on S_- for $A \leq 0$. Recall that Best's level set 25 in Fig. 1, which corresponds to phase $\vartheta = 0.49$, appears to come very close to itself after re-entering from the top of the figure, when sharply turning right to approach the hatched region. In Fig. 2, we show one additional primary level curve, labeled $L^\times$, which is not a simple curve, but contains a point, labeled p, where four local branches connect. This critical point p lies at $(\vartheta_o, A) \approx (0.5463, 3.4566)$.

We computed $L^\times$ in the region with $A \geq 0$ and determined its phase as $\vartheta \approx 0.5089$. Note that $L^\times$ bounds a region above it without isochrons in Figs. 1 and 2; its significance is discussed in detail in Section 5.1.

3.2 Accumulation of the level sets on the singular sets

Figures 1 and 2 feature regions in the (ϑ_o, A)-plane where the level sets L_ϑ are very close together and difficult to distinguish. In particular, Best was unable to determine the structure locally near S and S_-. Figure 3 illustrates how our method of direct computation resolves the intricate manner in which the primary level curves accumulate on the boundaries of these two regions of oscillator death.

Figure 3(a) is an enlargement showing 100 computed primary level curves as they approach S_-; the phases are again uniformly distributed and distinguished according to the color bar. The accumulation limit appears to be a closed, smooth and simple curve, which forms the boundary ∂S_- of the shaded singular set S_- of oscillator death. As Best already speculates in [2], to some extent, the boundary of the phaseless set is formed by a saddle periodic orbit and its three-dimensional stable manifold; the latter intersects each of the two half-cylinders $\mathcal{C}_\mathbf{d}$ and $\mathcal{C}_{-\mathbf{d}}$ in a single topological circle, giving rise in the (ϑ_o, A)-plane to the boundary curves ∂S and ∂S_-, respectively. A noticeable feature of Fig. 3(a) is that the level curves have a series of sharp, hooked turns as they accumulate on ∂S_-. Similar hooked turns were first observed in [30], where they were called 'boomerang turns', as a geometric feature of the one-dimensional isochrons in a planar reduction of the Hodgkin–Huxley model. Hence, it is perhaps not surprising to see similar hooked turns in the one-dimensional level sets of the three-dimensional isochrons for the Hodgkin–Huxley model (8). They reflect the way in which the three-dimensional isochrons accumulate on a thee-dimensional part of the basin boundary, formed by the stable manifold of the saddle periodic orbit. In [24], it was shown that hooked turns of the isochrons in planar systems arise from a strong difference in timescales.

Figure 3(b) and the enlargement in panel (c) illustrate how the representative level set $L_{0.55}$, which comprises a single, primary level curve, approaches the singular set. Panel (b) shows how $L_{0.55}$ approaches S for $A \geq 0$ and S_- for $A \leq 0$; the inset panel (c) shows an enlargement near S_- where the geometric features of $L_{0.55}$ are easier to see. We view this level curve as comprising two branches starting from $(\vartheta_o, A) = (0.55, 0)$: a positive one for $A \geq 0$, corresponding to $\mathcal{C}_\mathbf{d}$ and a negative one for for $A \leq 0$, corresponding to$\mathcal{C}_{-\mathbf{d}}$. Note that we are showing here the ϑ_o-range $[-0.1, 0.6]$ and extended the positive A-range, so that $L_{0.55}$ is a single curve. Observe how both branches make regularly occurring hooked turns, with extremely high and even increasing curvature, as they accumulate on ∂S_- and ∂S, respectively; the first hooked turn for the positive branch occurs at $(\vartheta_o, A) \approx (0.5855, 128.2199)$ and for the negative branch at $(\vartheta_o, A) \approx (0.9344, -44.4684)$. At these points, each branch changes direction and appears to 'retrace' its path, meaning that it passes so close to itself that the different segments are indistinguishable in the figure. At the second sharp turn, the respective branch changes direction again, and so on — winding ever tighter onto itself and featuring more and more hooked turns as it accumulates on the boundary of the respective singular set; see Fig. 3(c). Note from panels (a) and (b) that the positive branch winds around S in an clockwise direction, while the negative branch approaches ∂S_- anti-clockwise.

Since our method computes the primary level curve in L_ϑ in the (ϑ_o, A)-plane as a curve parameterized by arclength ℓ from its base point $(\vartheta_o, 0)$, we can distinguish each hooked turn by plotting $L_{0.55}$ as a function of ℓ. Figure 3(d1) is a three-dimensional view of the negative branch of $L_{0.55}$ in (ℓ, ϑ_o, A)-space, and panel (d2) shows its projection onto the (ℓ, A)-plane. Even though the negative branch of $L_{0.55}$ lies in a box in the (ϑ_o, A)-plane of size 0.4×50, the arclength of this

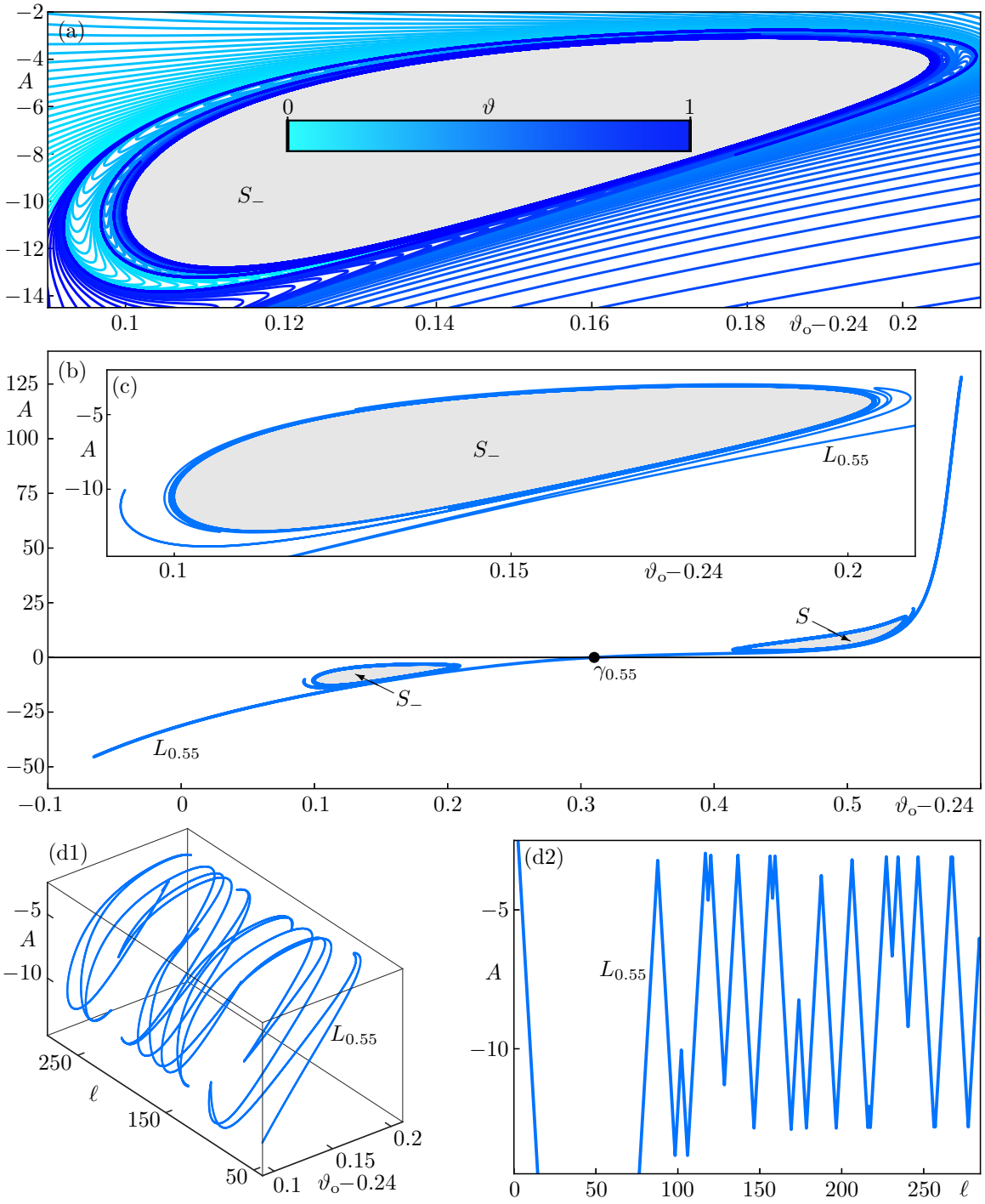

Figure 3: Accumulation of level sets in the (ϑ_o, A)-plane. Panel (a) is an enlargement of 100 uniformly distributed primary level curves near S_-, and panel (b) shows $L_{0.55}$ with both S_- and S; the singular sets are shaded gray, the level curves are colored according to phase from cyan to dark blue indicated by the color bar, and the inset panel (c) shows the same enlargement as in panel (a). Panels (d1) and (d2) show $L_{0.55}$ for $A \leq 0$ as a function of the arclength ℓ from $\gamma_{0.55}$ in (ℓ, ϑ_o, A)-space and in projection onto the (ℓ, A)-plane, respectively.

computed segment is well over 500. Observe in panels (c), (d1) and (d2) how the hooked turns occur as a regular and structured sequence of consecutive 'angular positions' with respect to the center of S_-.

4 Critical level sets and isochrons in planar examples

In order to explain the overall geometry of the level sets of the four-dimensional Hodgkin–Huxley model, we find it useful to consider first how critical isochrons and associated critical points of graph($\mathcal{P}_{\mathbf{d}}$) arise in planar systems. The case of planar systems is special, because the level sets have the same dimension as the isochrons themselves. However, we should still view them as intersection sets: our definition $L_\vartheta = \Upsilon_{\mathbf{d}}^{-1}(I_\vartheta \cap \mathcal{C}_{\mathbf{d}})$ still holds for any resetting direction $\mathbf{d} \in \mathbb{S}^1 \subset \mathbb{R}^2$. On the other hand, the attainable half-cylinder $\mathcal{C}_{\mathbf{d}}$ is not well defined in terms of a parameterization with respect to $\vartheta_{\mathrm{o}} \in [0, 1)$ and $A \geq 0$. Indeed, in the planar case, $\mathcal{C}_{\mathbf{d}}$ is collapsed to a half-strip, and a large segment of the set $\Upsilon_{\mathbf{d}}(\cdot, 0) = \Gamma$ lies in the interior of this half-strip. Consequently, there are (many) points in $\mathcal{C}_{\mathbf{d}}$ for which the perturbation map $\Upsilon_{\mathbf{d}}$ no longer has a unique inverse. More precisely, in the phase plane, each isochron I_ϑ can be viewed as having two branches, one *ingoing branch* that lies entirely inside Γ and one *outgoing branch* that lies entirely outside Γ. As we explain in more detail below, only the ingoing branch has a unique preimage under $\Upsilon_{\mathbf{d}}$, while the outgoing branch typically has two preimages. However, this property is not relevant in the context of how critical isochrons and associated critical points arise. We explain the overall geometry by considering two specific examples: a simple planar model due to Winfree, with rotational symmetry about the origin and explicitly known isochrons, and the FitzHugh–Nagumo model.

4.1 Winfree's planar model with a hole

Winfree constructed a number of planar models in the 1970s that have the unit circle as the attracting periodic orbit and are invariant under rotation about the origin, which is an equilibrium; see [35, 36]. In the same spirit, we consider the planar system given in polar coordinates by

$$\left\{ \begin{array}{rcl} \dot{r} & = & (1-r)(r-a)r, \\ \dot{\psi} & = & -(1+\omega(1-r)). \end{array} \right. \tag{10}$$

which, when written in Euclidean coordinates, takes the form

$$\left\{ \begin{array}{rcl} \dot{x} & = & \left(1-\sqrt{x^2+y^2}\right)\left(x\left(\sqrt{x^2+y^2}-a\right)+\omega\, y\right)+y, \\ \dot{y} & = & \left(1-\sqrt{x^2+y^2}\right)\left(y\left(\sqrt{x^2+y^2}-a\right)-\omega\, x\right)-x. \end{array} \right. \tag{11}$$

Since the equation for r in (10) does not depend on ψ, system (11) is invariant under rotation about the origin, which is the only (and stable) equilibrium $\mathbf{x}_s$. We study this model for the fixed choice of parameters $a = 0.25$ and $\omega = -0.5$, for which the unit circle is an attracting periodic orbit Γ and has period $T_\Gamma = 2\pi$; compare with [24, Sec. 3], where we used the same model. Additionally, the circle with radius $r = a$ is a repelling periodic orbit Γ_{u}, which surrounds $\mathbf{x}_s$. Hence, Γ_{u} forms the boundary of the basin of attraction $\mathcal{B}(\Gamma)$ of Γ, and the (closed) disk of radius a is the phaseless set. Perturbations into this 'hole' result in the loss or 'death' of the oscillations.

We choose $(x, y) = (1, 0)$ as the standard reference point $\gamma_0 \in \Gamma$ with zero phase. Following Winfree [36], the special form of (10) allows one to find the isochron I_ϑ of Γ for any given $\vartheta \in \mathbb{S}^1$ in terms of the dependence of ψ on the radius $r > a$, given by

$$\psi(r) = 2\pi \left(\frac{\omega}{2\pi a} \left[\ln\left(\frac{r}{r-a}\right) - \ln\left(\frac{1}{1-a}\right) \right] - \vartheta \right). \tag{12}$$

Hence, the isochron I_ϑ in the (x, y)-plane is given by

$$I_\vartheta = \left\{ (x, y) = (r\cos(2\pi\,\psi(r)), r\sin(2\pi\,\psi(r))) \in \mathbb{R}^2 \;\middle|\; r > a \right\}. \tag{13}$$

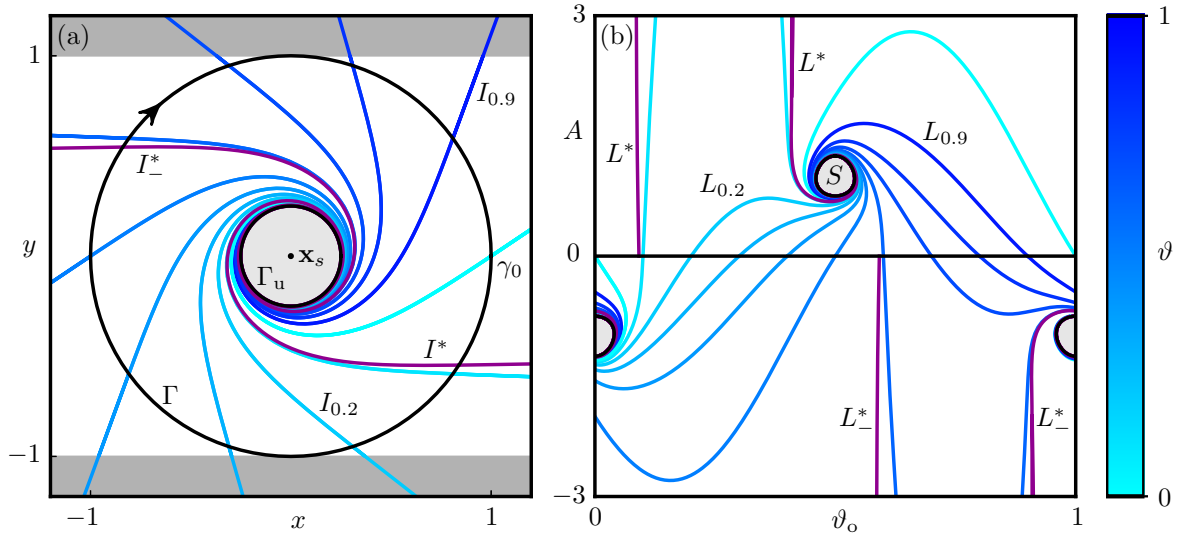

Figure 4: Phase resetting for the planar system (11) in the directions $\pm\mathbf{d} = (\pm 1, 0)^{\mathrm{T}}$. Panel (a) shows the (x, y)-plane with Γ and ten of its isochrons uniformly distributed in phase (indicated according to the color bar), together with Γ_{u}, which bounds the phaseless set (light-gray shading) that contains $\mathbf{x}_s$; the region with $|y| > 1$ (dark-gray shading) is not covered by translates of Γ along $\mathbf{d}$. Panel (b) shows the level sets of graph$(\mathcal{P}_{\mathbf{d}})$ for these same ten phases, together with the singular sets (light-gray shading) bounded by the images of Γ_{u} in the $(\vartheta_{\mathrm{o}}, A)$-plane. Also shown as purple curves in these two panels are the two critical isochrons I^* and I^*_- with associated critical level sets L^* and $L*_-$, respectively.

Figure 4 illustrates the geometry of graph$(\mathcal{P}_{\mathbf{d}})$ of system (11) for the fixed perturbation direction $\mathbf{d} = (1, 0)^{\mathrm{T}}$. Panel (a) shows the attracting periodic orbit Γ in the (x, y)-plane with ten isochrons distributed uniformly over one period; they are colored according to their phases as indicated by the color bar. The ingoing branch of each of the isochrons accumulates inside Γ, in a clockwise spiraling fashion on the boundary Γ_{u} of the singular set. The outgoing branches, on the other hand, hardly show any spiraling. The region $|y| \leq 1$ is the strip corresponding to the collapsed cylinder $\mathcal{C}_{\mathbf{d}} \cup \mathcal{C}_{-\mathbf{d}}$. Since we now consider translates of Γ in the direction $\mathbf{d}$ for any $A \in \mathbb{R}$, the interior $|y| < 1$, is covered twice, while the two boundary lines defined by $|y| = 1$ are covered once. jAll other points in the (x, y)-plane, namely, those with $|y| > 1$, are not covered by translates of Γ in the direction $\mathbf{d}$. Note that all but two isochrons, eventually enter the region $|y| > 1$, as their outgoing branches spiral away from Γ. The exceptions are two 'critical' isochrons, labeled I^* and I^*_- (purple), that have horizontal asymptotes as $x \to \pm\infty$; more precisely, in the limit as I^* and I^*_- go to infinity, their tangents are equal to $\pm\mathbf{d}$. It follows from (12) that $I^* = I_{\vartheta^*}$ with $\vartheta^* := \frac{\omega}{2\pi a} \ln(1 - a) \approx 0.0916$; by symmetry, its symmetric counterpart I^*_- has phase $\vartheta^*_- := \vartheta^* - 0.5 \approx 0.5916$ (modulo 1).

Figure 4(b) shows the $(\vartheta_{\mathrm{o}}, A)$-plane with the resulting level sets of graph$(\mathcal{P}_{\mathbf{d}})$ that correspond to the ten isochrons in panel (a). Due to the rotational symmetry of system (11), the phase-resetting surface graph$(\mathcal{P}_{\mathbf{d}})$ is invariant under reflection about the line $A = 0$ followed by a phase shift of ϑ_{o} by 0.5 (modulo 1). There are two holes in panel (b), for positive and negative A, respectively, which are the phaseless set S bounded by the preimages of Γ_{u} under the perturbation maps $\Upsilon_{\pm\mathbf{d}}$ from the $(\vartheta_{\mathrm{o}}, A)$-plane to the (x, y)-plane. The shown level sets are, similarly, the preimages of the selected ten isochrons, and they spiral around these holes; specifically, counterclockwise for $A \geq 0$. Note that, for each $\vartheta \in [0, 1)$, the entire level set L_ϑ in the positive half of the

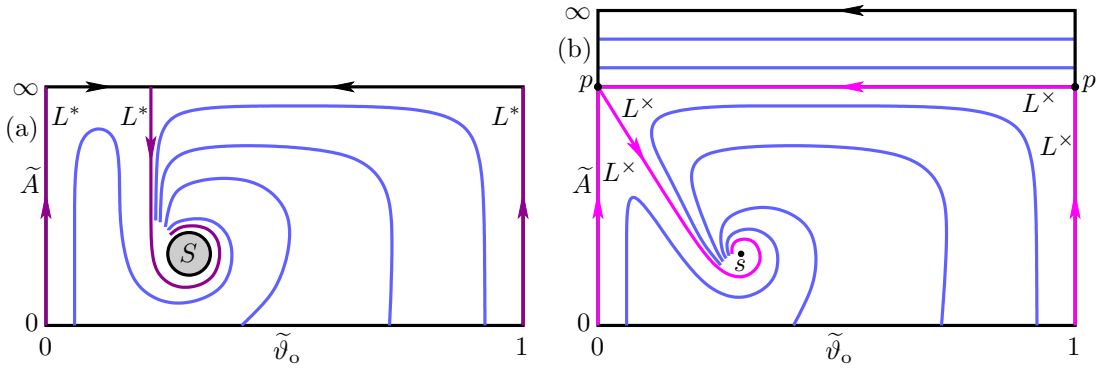

Figure 5: Sketches of the global geometry of level sets in the $(\widetilde{\vartheta}_o, \widetilde{A})$-rectangle representing the compactified (ϑ_o, A)-plane for systems (11) in panel (a) and (14) in panel (b). The top side of the rectangle represents $A = \infty$. Its left and right sides in panel (a) are formed by the component of L^* (purple) that connects to infinity; compare with Fig. 4(b). In panel (b), these sides are the component of $L^\times$ (magenta) from $(\vartheta_o, A) = (\vartheta, 0)$ to the critical point p, while the horizontal line through p in this representation corresponds to the non-contractible connecting loop of $L^\times$; compare with Fig. 6(b).

(ϑ_o, A)-plane, is mapped by $\Upsilon_{\mathbf{d}}$ to the isochron I_ϑ, but the image will only be the part of I_ϑ that lies in the double-covered strip. Furthermore, for each point on the outgoing branch of I_ϑ inside this double-covered strip, there are two preimages on L_ϑ. For example, the point $(x, y) = (1.3, 0)$, which lies on the edge of the frame in panel (a), can be reached by the two (ϑ_o, A)-pairs $(0, 0.3)$ and $(0.5, 2.3)$; therefore, these two very different points both lie on the same level set in panel (b). On the other hand, in panel (b), almost the entire part of $L_{0.9}$ in the positive half of the (ϑ_o, A)-plane has a unique image under $\Upsilon_{\mathbf{d}}$. Only the finite segment on $L_{0.9}$ from $(\vartheta_o, A) = (0.9, 0)$ to the point with $\vartheta_o = 0.75 - (0.9 - 0.75) = 0.6$ does not map one-to-one: starting from $(\vartheta_o, A) = (0.9, 0)$, points on $L_{0.9}$ first map to the outgoing branch of $I_{0.9}$, outside Γ, until the point on $L_{0.9}$ with $\vartheta_o = 0.75$, for which the corresponding point on $I_{0.9}$ has $y = 1$; the segment of $L_{0.9}$ from $\vartheta_o = 0.75$ to $\vartheta_o = 0.6$ maps again to this same part of the outgoing branch of $I_{0.9}$. We refer to A for an in-depth discussion with illustrations of this behavior.

Each of the level sets of graph$(\mathcal{P}_{\mathbf{d}})$ for system (11) consists of just the primary level curve; the only exceptions are the *critical level sets* L^* and L^*_- (purple) associated with I^* and I^*_-. Indeed, notice in Fig. 4(b) that the level set L_0 extends upwards and to the left from $A = 0$, while $L_{0.1}$ extends upwards and to the right; both have maxima and then spiral around S. Hence, there must be a special primary level curve that lies in between L_0 and $L_{0.1}$ and extends all the way to infinity without moving right or left. This primary level curve is one of the preimages under $\Upsilon_{\mathbf{d}}$ of the critical isochron I^*; therefore, it starts at the point $(\vartheta^*, 0) \approx (0.0916, 0)$. The other preimage of I^* forms a second component that comes from infinity and eventually spirals around S; hence, this second component of the critical level set L^* maps to both the outgoing and ingoing branches of I^*. By symmetry, the critical level set L^*_- is the preimage of I^*_- under the perturbation map $\Upsilon_{-\mathbf{d}}$. Both L^* and L^*_- are also shown in Fig. 4(b).

To illustrate the geometry of the level sets, we show a sketch in Fig. 5(a), where the (ϑ_o, A)-plane has been transformed to a rectangle with new 'idealized' coordinates $\widetilde{\vartheta}_o$ and $\widetilde{A}$. In this representation, $A \geq 0$ has been compactified (for example, by stereographic projection) to $\widetilde{A} \in [0, 1]$, so that the upper boundary in Fig. 5(a) represents $A = \infty$. Furthermore, the horizontal coordinate $\widetilde{\vartheta}_o$ represents a (nonlinear) transformation of ϑ_o so that the left and right sides of the rectangle correspond to the component of L^* (purple) that extends from $A = 0$ all the way to

$A = \infty$ and, hence, connects the bottom and top boundaries of the shown rectangle. In essence, the parameterization $\mathbb{S}^1 \times \mathbb{R}_0^+$ of the half-cylinder $\mathcal{C}_\mathbf{d}$ has been cut along L^* and then rescaled and compactified. Such a coordinate transformation exists, because all isochrons are transverse to Γ, that is, to the bottom boundary with $\widetilde{A} = 0$. Notice the second component of I^* that extends from $A = \infty$ and spirals around the singular set S; compare with Fig. 4(b). As Fig. 5(a) shows, the complement of $I^* \cup S$, which is a simply connected open set, is foliated by the family of preimages of the isochrons I_ϑ with $\vartheta \in \mathbb{S}^1 \setminus \vartheta^*$. The geometry of the level sets for system (11) is representative for the case that there is no critical point with finite A, and the two components of the critical level set connect at ∞.

4.2 The FitzHugh-Nagumo system with a shift

We now consider the FitzHugh–Nagumo system [13, 29], which we write in the form

$$\left\{ \begin{array}{rcl} \dot{x} &=& c\,(y + x - \frac{1}{3}\,x^3 + z), \\ \dot{y} &=& -\frac{1}{c}\,(x - a + b\,y). \end{array} \right. \tag{14}$$

As in [26], we fix $a = 0.7$ and $b = 0.8$ and consider the case $c = 1$ with practically no time-scale separation between x and y; moreover, we set $z = -0.8$ so that the equilibrium is shifted and no longer at the origin. For this choice of parameters, system (14) has the attracting periodic orbit Γ with clockwise motion, which surrounds the repelling focus equilibrium $\mathbf{x}_\mathrm{u} \approx (0.2729, 0.5339)$; hence, the phaseless set is a single point in this case.

In contrast to system (11) with its rotational symmetry, the FitzHugh–Nagumo system (14) is a typical planar example in the sense that its isochrons are not given in explicit form. Nevertheless, the isochrons and level sets of the function $\mathcal{P}_\mathbf{d}$ can be computed reliably with a boundary value problem setup and they are shown in Fig. 6. The situation in the (x, y)-plane is shown in panel (a). The zero-phase point with maximum value of the x-coordinate lies at $\gamma_0 \approx (0.9660, 0.1345) \in \Gamma$. The isochrons, of which 50 are shown colored according to their phases in light shades of blue, spiral clockwise into the single phaseless point $\mathbf{x}_\mathrm{u}$; this is due to the period $T_\Gamma \approx 10.8329$ of Γ being smaller than the rotation period around the focus $\mathbf{x}_\mathrm{u}$ with eigenvalues $0.0628 \pm 0.5056\,i$.

We consider again perturbations in the direction $\mathbf{d} = (1, 0)^\mathrm{T}$ only, as defined by the perturbation map $\Upsilon_\mathbf{d}$. Hence, the translates of Γ form a (collapsed) attainable half-cylinder (white strip), given as range($\Upsilon_\mathbf{d}$). As mentioned before, only the region bounded by Γ in Fig. 6(a) is covered once, as are the bounding top and bottom horizontal straight lines at the maximal and minimal y-values of Γ; the interior of range($\Upsilon_\mathbf{d}$) outside Γ is covered twice. Panel (b) shows the corresponding level sets of graph($\mathcal{P}_\mathbf{d}$) in the $(\vartheta_\mathrm{o}, A)$-plane; the level sets are colored with a gradient from cyan to dark blue according to their heights on the phase-resetting surface. Each level set L_ϑ is the preimage of I_ϑ under the perturbation map $\Upsilon_\mathbf{d}$, which is only defined for the part(s) of I_ϑ that lie(s) in the attainable half-cylinder. The primary level curves are all well-defined curves locally near $A = 0$. Note that almost all primary level curves spiral into the singular point labeled s, which is the (unique) preimage $\Upsilon_\mathbf{d}^{-1}(x_u)$. The only exception is the critical set $L^\times = L_\vartheta$ (magenta) with $\vartheta \approx 0.0777$: its primary level curve ends at the critical point $p \approx (0.1119, 0.2286)$, a point where four local branches connect; the critical point p is, hence, a saddle point of graph($\mathcal{P}_\mathbf{d}$). Note that two local branches of $L^\times$ near p connect globally to form a single non-contractable curve, which is the upper boundary of the region with level sets that spiral into s. Level sets L_ϑ have additional, disjoint components that lie above this curve $L^\times$; these additional level curves are all non-contractible, closed curves of the parameterization by ϑ_o and A on $\mathbb{S}^1 \times \mathbb{R}_0^+$.

Figure 6(a) shows the critical isochron $I^\times = I_\vartheta$ (magenta) with $\vartheta \approx 0.0777$ associated with $L^\times$. It is characterized by the property that it has a tangency point t with the boundary line

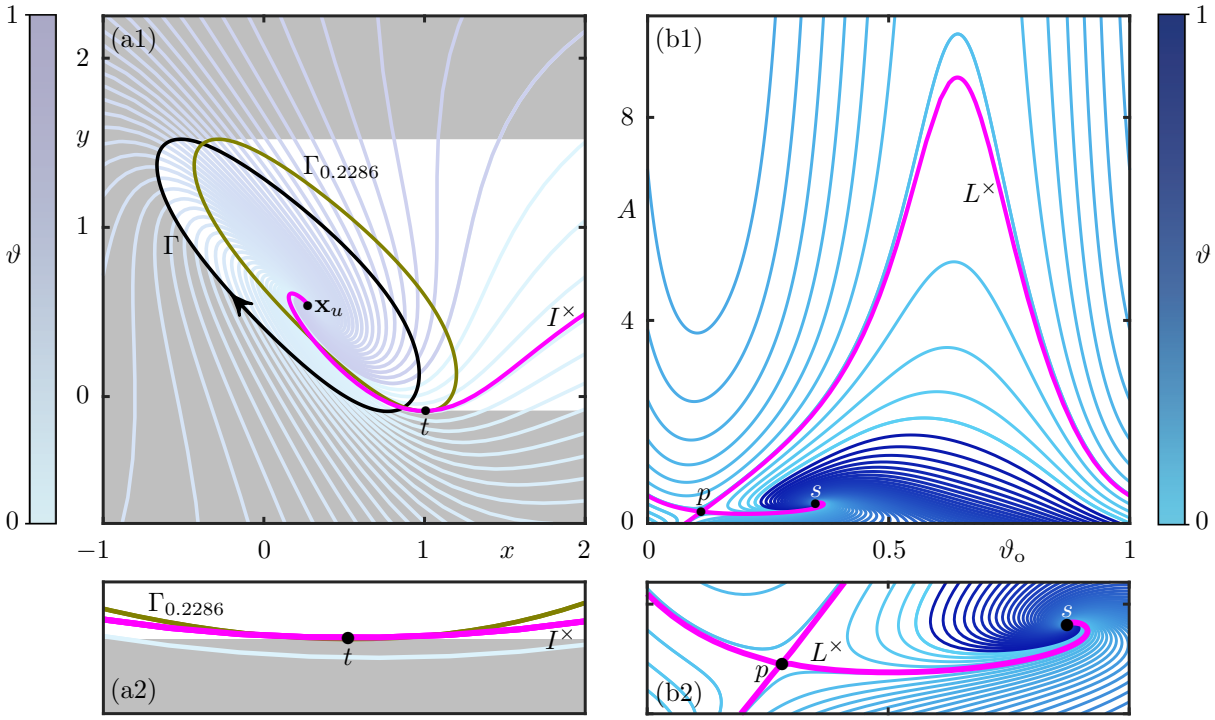

Figure 6: Structure of the isochrons and corresponding level sets for perturbations of the FitzHugh–Nagumo system (14) in the direction $\mathbf{d} = (1, 0)^T$. Panel (a) shows the (x, y)-plane with Γ, the phaseless point $\mathbf{x}_u$, and 50 isochrons that are uniformly distributed in phase ϑ as indicated by the color bar. Also shown are the image of $\Upsilon_\mathbf{d}$ (white), its complement (gray shading), the critical isochron $I^\times = I_\vartheta$ with $\vartheta \approx 0.0777$ that has a tangency point t with the lower boundary of range$(\Upsilon_\mathbf{d})$, and the associated critical perturbation set $\Gamma_{0.2286}$ that contains t for $\vartheta_o \approx 0.1119$. Panel (b) shows the corresponding 50 level sets of graph$(\mathcal{P}_\mathbf{d})$ in the (ϑ_o, A)-plane, as well as the critical level set $L^\times = L_\vartheta$ with $\vartheta \approx 0.0777$ that contains the critical point $p \approx (0.1119, 0.2286)$.

of range$(\Upsilon_\mathbf{d})$; specifically, the tangent of $I^\times$ at t is $\mathbf{d}$ and t has the minimal possible y-value of range$(\Upsilon_\mathbf{d})$. Also shown is the unique perturbation set $\Gamma_{0.2286}$ that contains t, namely as the point with $\vartheta_o \approx 0.1119$. The preimage of the boundary tangency point t is exactly the critical point p, and it identifies the critical isochron $I^\times$ whose preimage under $\Upsilon_\mathbf{d}$ is the critical level set $L^\times$.

The phase-resetting surface graph$(\mathcal{P}_\mathbf{d})$ itself is shown in Fig. 7 over the (ϑ_o, A)-plane with $A \in [0, 3]$. In order to illustrate its structure, we show the surface with additional lifted copies over the extended range $[-1, 2]$ of the periodic variable ϑ_n; moreover, we show the lifts of the 50 level sets from Fig. 6(b), from which this surface was rendered. Notice in Fig. 7 how graph$(\mathcal{P}_\mathbf{d})$ scrolls around the singular vertical line s, which is due to the spiraling of the isochrons around the phaseless set $\mathbf{x}_u$ [27, 26]. Also shown are the two relevant lifts of the critical level set $L^\times$ with the point p of graph$(\mathcal{P}_\mathbf{d})$. Observe that p is indeed a saddle point: from the chosen viewpoint in Fig. 7, the surface goes upwards to the far left and near right of $L^\times$, and down in the complementary two sectors.

We complete this section by pointing out that $L^\times$ in Fig. 6(b) plays the same role as the critical level set L^* in Fig. 4(b) together with infinity. This is illustrated by the sketch in Fig. 5(b) in the associated rescaled $(\widetilde{\vartheta}_o, \widetilde{A})$-rectangle. More specifically, the branches from $A = 0$ to the point p and from p to the singular set s in Figs. 6(b) and 5(b) act as the two branches of L^* in Figs. 4(b) and 5(a), while the non-contractible loop from p back to itself plays the role of boundary of the region with primary level curves that accumulate on the singular set. To emphasize this

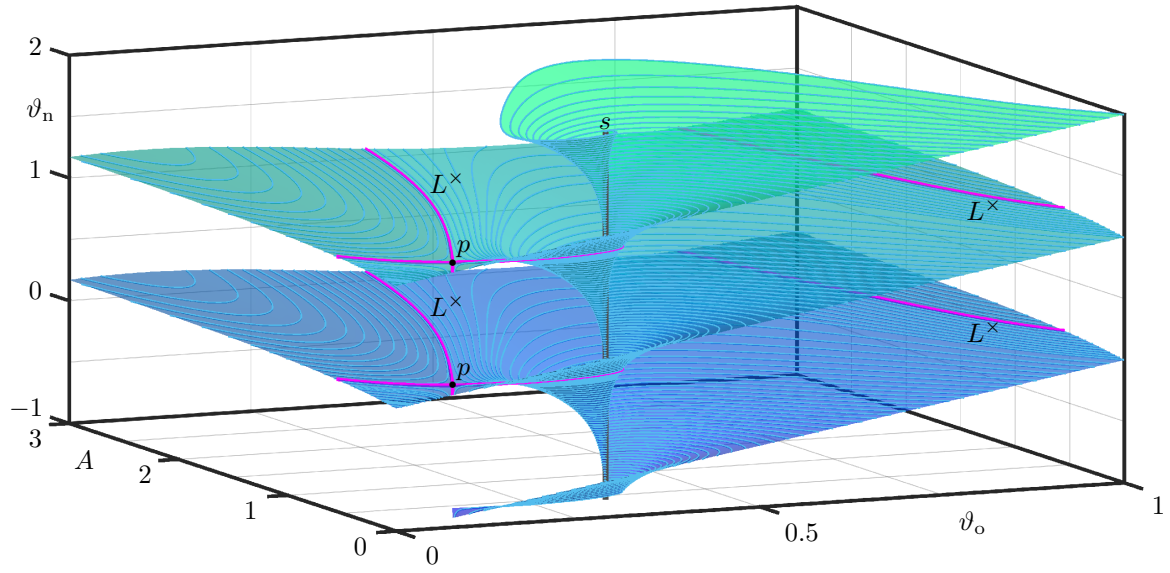

Figure 7: The phase-resetting surface graph($\mathcal{P}_\mathbf{d}$) of the FitzHugh–Nagumo system (14) with respect to the direction $\mathbf{d} = (1, 0)^\mathrm{T}$ shown in $(\vartheta_o, A, \vartheta_n)$-space for $A \in [0, 3]$ over the extended ϑ_n-range $[-1, 2]$. Also shown are the singular vertical line s, as well as the lifts of 50 computed level sets and of the critical level set $L^\times$ with the saddle point p. Compare with Fig. 6(b).

comparison, the loop has been 'straightened out' to a horizontal line in Fig. 5(b), which is shown at the same height as the upper boundary representing infinity $A = \infty$ in panel (a). Notice, in particular, that the branch from p to s divides the level curves that converge on s from the left and right, respectively. We conclude that the resetting surface graph($\mathcal{P}_\mathbf{d}$) of the FitzHugh–Nagumo system (14) features a saddle point p that exists for finite A, rather than one for infinite A, as is the case for the phase-resetting surface of system (11).

5 Overall level-set geometry of the Hodgkin–Huxley model

We now return to the four-dimensional Hodgkin–Huxley model (8) and discuss the overall structure of the level sets of graph($\mathcal{P}_\mathbf{d}$) with respect to the direction $\mathbf{d} = (1, 0, 0, 0)^\mathrm{T}$. To this end, we show in Fig. 8 the (ϑ_o, A)-plane over the A-range $[-100, 100]$ with 100 computed level sets L_ϑ that are uniformly distributed in ϑ and colored according to their phases as given by the color bar. This refinement in the number of level sets gives a better impression of how all but two of the primary level curves accumulate on S for $A \geq 0$ and on S_- for $A \leq 0$; compare with Fig. 2. Also shown in Fig. 8 in the region with $A \geq 0$ is the critical level set $L^\times$ with phase $\vartheta \approx 0.5089$ that contains the critical point p, which is a saddle. On this larger A-range, we see that two of the four branches of $L^\times$ that meet at p close up to enclose a region of the (ϑ_o, A)-plane with level curves that are smooth concentric closed loops. The 100 computed level sets shown in Fig. 8 include three such closed level curves; indeed, the previously 'empty' region of the (ϑ_o, A)-plane in Figs. 1 and 2 is filled with such closed level curves. Note this isola of concentric curves implies the existence of a second critical point. We found that these closed level curves surround the point $q \approx (0.3043, 28.2007)$, which is a local maximum of the phase-resetting surface graph($\mathcal{P}_\mathbf{d}$) with phase $\vartheta_n = \mathcal{P}_\mathbf{d}(q) \approx 0.2958$.

The geometry of the critical level set $L^\times$ for the Hodgkin–Huxley model (8) is similar to, but not the same as the critical level set $L^\times$ for the FitzHugh–Nagumo system (14). Namely, as is shown in Fig. 8, the two branches at p that connect now do so in a contractible loop that bounds

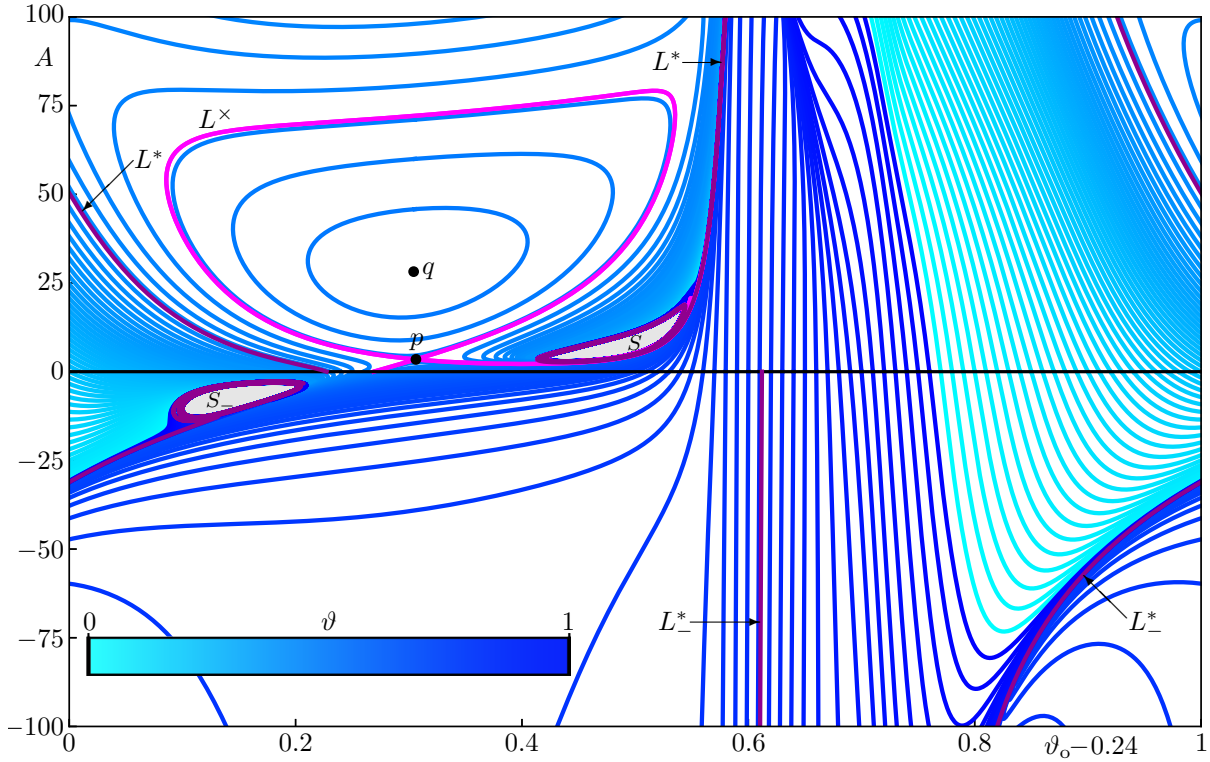

Figure 8: Level sets of graph($\mathcal{P}_\mathbf{d}$) for the Hodgkin–Huxley model (8) in the directions $\pm\mathbf{d} = (\pm 1, 0, 0, 0)^\mathrm{T}$. Shown over a larger A-range are 100 computed level sets with uniformly distributed phases as given by the color bar, the critical level set $L^\times$ (magenta), together with the critical points p and q (black dots), and the critical level sets L^* and L^*_- (purple); compare with Fig. 2.

the family of concentric curves. We discuss their properties in more detail in Section 5.1. The fact that the loop is contractible implies the existence of a second critical level set 'connecting to' and 'returning from' infinity, in much the same way as the critical level set L^* for Winfree's simply planar system (11); we explain this in detail in Section 5.2.

5.1 The isola of concentric level curves

All level sets L_ϑ for $A \geq 0$ with $\vartheta \in (\mathcal{P}_\mathbf{d}(p), \mathcal{P}_\mathbf{d}(q)) = (0.2689, 0.2958)$ have (at least) two components: the primary level curve from $(\vartheta_o, A) = (\vartheta, 0)$ that approaches ∂S and a closed level curve surrounding q. The closed loop of $L^\times$ bounds the region of concentric level curves. Since, q is a local maximum of $\mathcal{P}_\mathbf{d}$, this region corresponds to a 'local hill' of the phase-resetting surface graph($\mathcal{P}_\mathbf{d}$). Note that this hill is very shallow since the difference in $\mathcal{P}_\mathbf{d}$ between $L^\times$ and q is less than 0.03.

Figure 9 illustrates the region or isola of concentric level curves. Panel (a) is effectively an enlargement of Fig. 8 that shows $L^\times$, p, q, and S in the (ϑ_o, A)-plane, but now with 26 concentric level curves in L_ϑ for equally distributed ϑ; other level curves are not shown for clarity. Panels (b)–(d) show these concentric level curves on the actual half-cylinder $\mathcal{C}_\mathbf{d} \subset \mathbb{R}^4$ projected onto the (V, m)-plane, the (V, n)-plane, and the (V, h)-plane, respectively. This representation shows the local intersections sets of $\mathcal{C}_\mathbf{d}$ with the corresponding three-dimensional isochrons. Note, however, that the projection of $\mathcal{C}_\mathbf{d}$ onto a plane of system variables causes a large region to be covered twice, similar to the planar situation we discussed in Sections 4.1 and 4.2.

The projection onto the (V, m)-plane in Fig. 9(b) is a diffeomorphic image of what one sees

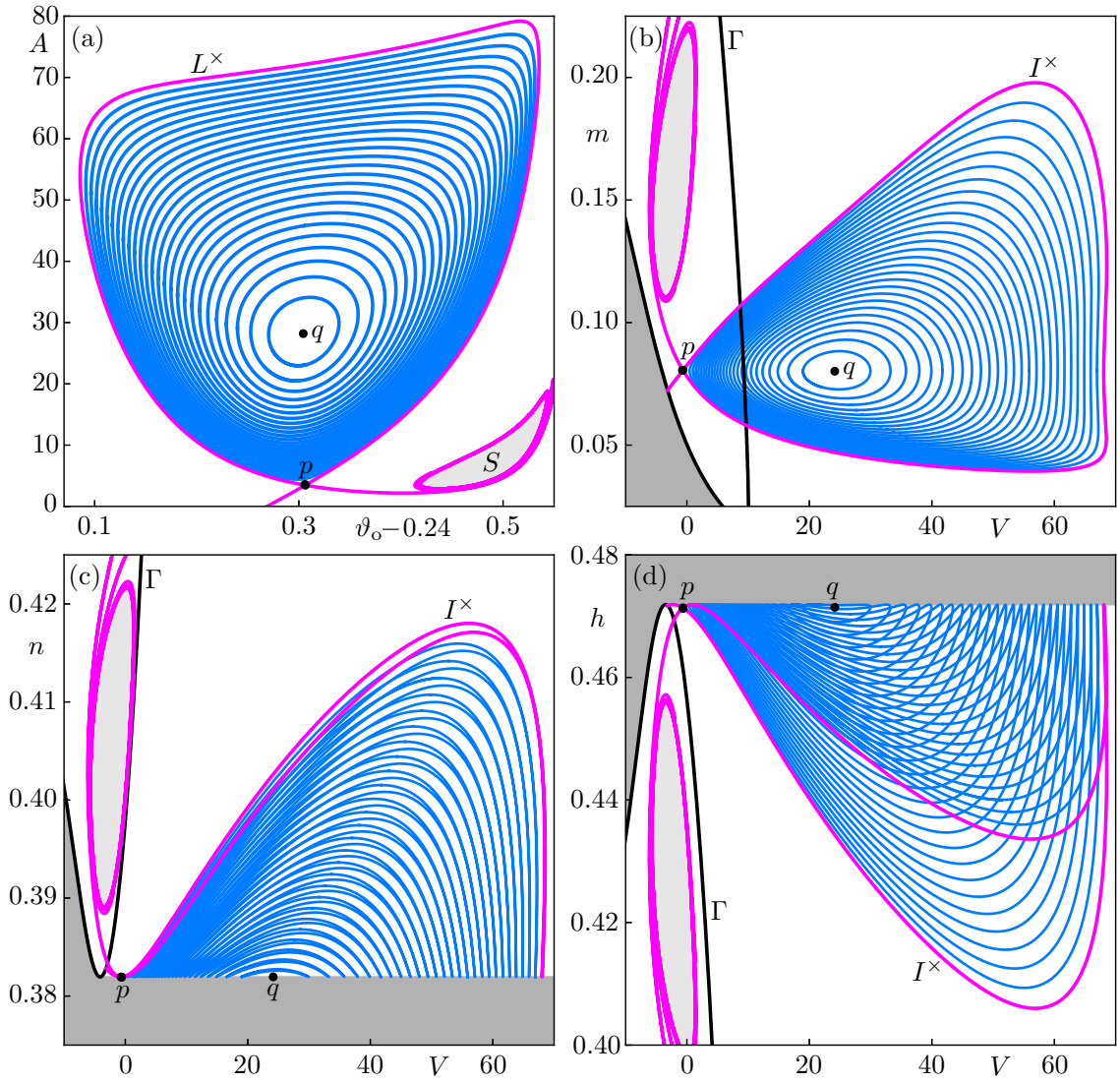

Figure 9: Concentric level curves and corresponding intersection curves of isochrons. Panel (a) shows the (ϑ_o, A)-plane with L_ϑ for $\vartheta = 0.51 + j * 0.01$ and $j = 0, ..., 25$, the critical level set $L^\times$ (magenta curve), the critical points p and q (black dots), and the singular set S (light-gray shading). Panels (b)–(d) shows the corresponding intersection sets on $\mathcal{C}_\mathbf{d}$, together with segments of Γ (black curve), in projection onto the (V, m)-plane, the (V, n)-plane, and the (V, h)-plane, respectively; here, the region outside the (projection of) the attainable half-cylinder $\mathcal{C}_\mathbf{d}$ is shaded gray.

in the (ϑ_o, A)-plane. However, the projections of $\mathcal{C}_\mathbf{d}$ in panels (c) and (d) onto the (V, n)-plane and the (V, h)-plane, respectively, 'fold over' the closed intersection curves because the saddle point p is practically on the boundary of the respective strip of projected $\mathcal{C}_\mathbf{d}$. In these two projections, almost all closed curves have two tangency points on the boundary of the strip because the maximum q also lies almost on the boundary of the respective strip. Note that the closed curves in panel (c) are almost single arcs. As Fig. 9 illustrates, it is difficult to appreciate the geometric structure based on a single planar projection of $\mathcal{C}_\mathbf{d} \subset \mathbb{R}^4$. Indeed, in contrast to the planar case, there is no unique, natural projection of $\mathcal{C}_\mathbf{d}$ onto $\mathbb{R}^2$.

Recall that, by definition, all level sets, including the critical points p and q, correspond to intersection sets of isochrons with the cylinder $\mathcal{C}_\mathbf{d}$. What is special about p and q is that the

associated isochrons have three-dimensional tangent spaces at these points that contain the planes tangent to $\mathcal{C}_{\mathbf{d}}$ at these points. Hence, they are points where the Jacobian of $\mathcal{P}_{\mathbf{d}}$ is singular, and p and q are distinguished by the Hessian. While $\mathcal{P}_{\mathbf{d}}$ is not given by an explicit formula, our calculations suggest that p is a minimum and q a maximum of $\mathcal{P}_{\mathbf{d}}$ in the direction $\mathbf{d}$. Moreover, both p and q are local maxima of $\mathcal{P}_{\mathbf{d}}$ in the direction perpendicular to $\mathbf{d}$, meaning that p is indeed a saddle point and q a local maximum of graph($\mathcal{P}_{\mathbf{d}}$). More precisely, the tangent plane of $\mathcal{C}_{\mathbf{d}}$ at p is contained in the tangent space of the isochron $I_{0.2689}$ at p; relative to this tangent plane, p is a critical point of saddle type. The same is true for the isochron $I_{0.2958}$ and the critical point q at the center of the concentric level sets; relative to the tangent plane, q is a maximum.

5.2 The critical level sets L^* and L^*_-

We now return to the discussion of global aspects of the foliation of the (ϑ_o, A)-plane by level sets. While the 'empty region' for $A \geq 0$ in Figs. 1 is due to a 'shallow hill' that Best was not able to resolve, the seemingly empty region for $A \leq 0$ is different: Fig. 8 shows additional level curves that pass through this region; the level sets are quite far from each other, which means that the phase-resetting surface graph($\mathcal{P}_{\mathbf{d}}$) is almost constant here. However, there are no critical points on the cylinder $\mathcal{C}_{-\mathbf{d}}$, and this means that the level sets L_ϑ for $A \leq 0$ all consist of only the primary level curves that are continued from $(\vartheta_o, A) = (\vartheta, 0)$. This set of curves needs to foliate $\mathbb{S}^1 \times \mathbb{R}^+_0 \setminus S_-$, which is exactly the situation we encountered for the planar system (11) in Section 4.1: The presence of the singular set S_- implies that there must exist a critical level set L^*_- connecting to infinity, as shown in Fig. 4(b) and sketched in Fig. 5(a); it separates the level sets that initially curve away from $A = 0$ to the left and those that curve to the right. Recall that the level sets must foliate the entire basin, which means they must also all extend arbitrarily close to infinity. We computed a sufficiently long part of L^*_- by continuation from $A = 0$ as a level set that turns neither left nor right up to a very large value of A. In this way we found $L^*_- = L_\vartheta$ with $\vartheta \approx 0.6120$, which is the practically straight vertical line in the bottom half of Fig. 8. The part of L^*_- 'returning from infinity' is then found by continuation in ϑ for fixed A from a nearby already computed level set; it is subsequently continued as a curve for fixed $\vartheta = 0.6120$ and also shown in Fig. 5(a). Note how this second level curve in L^*_- enters the shown frame at about $\vartheta_o = 0.82$ and then accumulates on S_-. All other level curves approach this second part of L^*_- from the left and right, respectively, and exhibit quite sharp turns in the process. All level sets, including L^*_-, approach S_- by performing hooked turns, but otherwise the overall structure in the (ϑ_o, A)-plane is as sketched in Fig. 5(a).

The intersection structure on $\mathcal{C}_{\mathbf{d}}$ gives rise to the isola of concentric level curves bounded by the connecting loop of the critical level set $L^\times$. Hence, it may seem that this is much like the foliation by level sets we found for the planar FitzHugh–Nagumo system (14), as shown in Fig. 6(b1) and sketched in Fig. 5(b). However, this is not the case due to an important difference in the topological nature of the branch of level set $L^\times$ connecting p to itself. As we already mentioned in Section 5.1, the critical level set for the planar FitzHugh–Nagumo system is non-contractible on $\mathbb{S}^1 \times \mathbb{R}^+_0 \setminus S$; consequently, the primary level curves continued from $(\vartheta_o, A) = (\vartheta, 0)$ only foliate the finite region below this connecting curve; see Fig. 6(b1). For the four-dimensional Hodgkin–Huxley model, on the other hand, the connecting loop to p in the critical level set $L^\times$ is contractible, namely to the critical point q via the family of concentric curves surrounding it; see 9(a). This means that the level curves in L_ϑ that are continued from $(\vartheta_o, A) = (\vartheta, 0)$ for $A \geq 0$ must foliate the unbounded region of the (ϑ_o, A)-plane outside S and outside the isola of concentric level sets bounded by the connecting loop to p, which is also a closed (topological) disk. Hence, the family of primary level curves must also get arbitrarily close to infinity, in the same

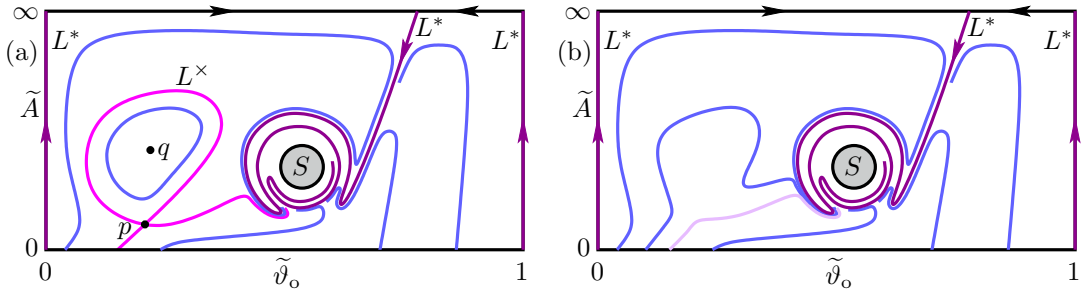

Figure 10: Sketch of the foliation by level sets encountered in the Hodgkin–Huxley model (8) for the direction $\mathbf{d} = (1, 0, 0, 0)^{\mathrm{T}}$, shown in the style of Fig. 5(a) in the compactified $(\widetilde{\vartheta}_o, \widetilde{A})$-rectangle. Panel (a) represent the situations for $A \geq 0$ with $L^\times$ (magenta), p, q, L^* and S, and panel (b) that for $A \leq 0$ with only L^* and S, with a level curve (light magenta) that is about to undergo a cubic tangency in the direction $\mathbf{d}$. Compare with Fig. 8.

way as is the case for $A \leq 0$ on outside S_-. Therefore, there also exists a critical level set L^* for the region $A \geq 0$, which we identified as $L^* = L_\vartheta$ with $\vartheta \approx 0.2274$. Specifically, we computed L^* in the same way as L^*_- by finding a primary level curve that 'keeps going to infinity' in the sense that it does not have a turning point with respect to A, up to a very large value of A. Its two branches are shown in Fig. 8. They are topologically as the branches of L^*_-, but there are geometrical differences: the branch of L^* from $(\vartheta_o, 0) = (0.2274, 0)$ is definitely not a vertical line, while the branch coming back from infinity enters the frame almost vertically.

We finish this section by presenting, in Fig. 10, sketches in the rescaled and compactified $(\widetilde{\vartheta}_o, \widetilde{A})$-rectangle of the foliations by level sets that we encountered for the phase-resetting surface of the Hodgkin–Huxley model (8) for the directions $\pm\mathbf{d} = (\pm 1, 0, 0, 0)^{\mathrm{T}}$. Panel (a) shows the foliation of the complement of S with the critical level sets $L^\times$ and L^* that organise the foliation of the (ϑ_o, A)-plane. In the style of Fig. 5, the upper boundary represents $A = \infty$ and the left and right boundaries are the branch of L^* that connects to infinity. A small number of additional level sets illustrate the nature of the overall foliation, where the development of the hooked turns as S is approached is also sketched.

As was discussed in Section 5.1, the connecting loop of $L^\times$ is contractible. In fact, this contraction can likely be achieved either by changing a parameter of the Hodgkin–Huxley model, or by changing the direction vector $\mathbf{d}$ in such a way that the critical points p and q move closer together and then disappear at a cubic tangency. Subsequently, the foliation will no longer feature critical points nor the critical level set $L^\times$. This situation is sketched in Fig. 10(b), where one of the level curves (light magenta) is about to undergo a cubic tangency in the direction $\mathbf{d}$. Note that this case is qualitatively the foliation on we found for the Hodgkin–Huxley model (8) for $A \leq 0$ in Fig. 8. While it is topologically as Fig. 5(a), the sketch in Fig. 10(b) illustrates that the 'empty region' for $A \leq 0$ left unexplored by Best in Fig. 1 appears to be due to a closeness to a cubic tangency. When a system parameter or $\mathbf{d}$ is changed slightly one would expect to see the appearance of a saddle, and a maximum (or minimum) surrounded by concentric level curves, as is the case for $A \geq 0$.

6 Conclusions and outlook

We demonstrated that it is possible to compute level sets of the phase-resetting surface graph$(\mathcal{P}_\mathbf{d}(\vartheta_o, A))$ of an attracting periodic orbit Γ with respect to a given perturbation direction $\mathbf{d}$, irrespective of the

dimension m of the underlying continuous-time dynamical system. This is achieved by formulating the input-output relationship $\vartheta_\mathrm{n} = \mathcal{P}_\mathbf{d}(\vartheta_\mathrm{o}, A)$, between the phase ϑ_o at which the perturbation is applied, its amplitude A and the resulting phase ϑ_n, as a boundary value problem, which is then solved by collocation in combination with pseudo-arclength continuation. In this way, we are able to compute level sets L_ϑ, comprising one or more level curves, in the foliation of the $(\vartheta_\mathrm{o}, A)$-plane for a representative number of values of ϑ.

Our motivation has been the work of Eric Best in the 1970s, who sketched the level sets of the phase-resetting surface for the four-dimensional Hodgkin–Huxley model after performing simulations to obtain the new phase ϑ_n over a grid in the $(\vartheta_\mathrm{o}, A)$-plane. We computed the level sets directly, for up to 100 values of ϑ, and this allowed us to determine and illustrate their properties in unprecedented detail. We showed that the level sets perform very sharp or hooked turns as they accumulate on topological disks where ϑ_n is not defined. Moreover, we found two different kinds of critical levels sets: a level set $L^\times$ due to a saddle point in the $(\vartheta_\mathrm{o}, A)$-plane, and a level set L^* 'connecting to' and 'returning from' infinity. We clarified the nature of both these types of critical level sets with planar examples, and illustrated how they contribute to organizing the foliation in the $(\vartheta_\mathrm{o}, A)$-plane. In a nutshell, we 'completed' the image of Best and determined the overall geometry of the phase-resetting surface.

From a more general perspective, the level sets L_ϑ are effectively the intersection sets of the two-dimensional half-cylinder $\mathcal{C}_\mathbf{d}$ with the $(m-1)$-dimensional isochrons that foliate the basin of attraction $\mathcal{B}(\Gamma) \subset \mathbb{R}^m$ of Γ. As we discussed, for planar systems, the half-cylinder $\mathcal{C}_\mathbf{d}$ is collapsed and, hence, not uniquely parameterized by ϑ_o and A; in particular, the outgoing branches of the isochrons lie in the region that is covered twice by the perturbation map. In the higher-dimensional case, $\mathcal{C}_\mathbf{d}$ is a proper two-dimensional surface with only Γ as its boundary. Hence, typically, ϑ_o and A uniquely parameterize $\mathcal{C}_\mathbf{d}$; the exceptions are when $\mathbf{d}$ happens to be chosen parallel to a direction that connects two points in Γ: the simplest case is that Γ lies in a plane and $\mathbf{d}$ is parallel to this plane, which effectively embeds the planar system in a higher-dimensional setting; however, also for periodic orbits in general position, it is possible that one point, say, $\gamma_{\vartheta_1} \in \Gamma$ can be parameterized as $(\vartheta_1, 0)$, as well as (ϑ_2, A_2) for special choices of $\vartheta_2 \in [0, 1)$ and $A_2 > 0$. In this latter situation, the straight line $\{\vartheta = \vartheta_2\}$ on $\mathcal{C}_\mathbf{d}$ will be double-covered. Note that one would typically expect a finite number of double-covered straight lines (if any at all) for a periodic orbit $\Gamma \subset \mathbb{R}^m$ with $m \geq 3$ and chosen direction vector $\mathbf{d}$.

Computing level sets of the phase-resetting surface $\mathrm{graph}(\mathcal{P}_\mathbf{d}(\vartheta_\mathrm{o}, A))$ in the $(\vartheta_\mathrm{o}, A)$-plane is a way to learn about the geometry of higher-dimensional isochrons. In this regard, we mention that the vector $\mathbf{d}$ can be changed to 'drill' with the half-cylinder $\mathcal{C}_\mathbf{d}$ in different directions through the $(m-1)$-dimensional isochrons of Γ. Indeed, this procedure also identifies singular regions in the $(\vartheta_\mathrm{o}, A)$-plane where the new phase is not defined, so that information on the boundary of the basin $\mathcal{B}(\Gamma)$ is also obtained. Since this boundary is formed generically by $(m-1)$-dimensional and/or $(m-2)$-dimensional stable manifolds of saddle equilibria and saddle periodic orbits, the method we presented here is a novel way to probe these objects in phase spaces of dimension $m \geq 4$.

Acknowledgments

We thank Andrus Giraldo for his fruitful discussions surrounding the computational setup.

A Algorithm for computing level curves of the phase-resetting surface

We employ the quite general approach of tracing out a curve of interest by considering a one-parameter family of orbit segments obtained as solutions of a suitably defined multi-segment boundary value problem (BVP). This solution family is then computed with a collocation solver for the BVP in combination with pseudo-arclength continuation; see [22] for details and examples. In particular, this approach has been employed to continue one-dimensional isochrons as arclength-parameterized curves, even when they are very complicated geometrically [16, 17, 23, 24, 30]. Moreover, a BVP setup was presented in [25] to compute phase transition curves by continuation in systems of any dimension; see also [26, 27] for more examples. Here, we extend this technique to compute level curves of graph($\mathcal{P}_{\mathbf{d}}(\vartheta_{\mathrm{o}}, A)$) for systems with a state space of any dimension $m \geq 2$. More specifically, we find a particular level set in the $(\vartheta_{\mathrm{o}}, A)$-plane by computing the set of intersection curves of the two-dimensional half-cylinder $\mathcal{C}_{\mathbf{d}}$ with isochrons of dimension $m-1$.

The algorithm to compute level curves of the phase-resetting surface for a periodic orbit Γ with period T_Γ is based on the numerical method that we developed for computing a phase response curve [25, 27]. At its core is the six-segment BVP from [25] for the computation of phase transition curves of a planar system; we refer the interested reader to [25] for full details of the BVP setup. The higher-dimensional set-up for computing level curves in arbitrary dimensions essentially only differs in the choice of free and fixed parameters of the problem. The method is implemented in the unix/linux software package Auto-07P [8, 9] as well as the Matlab-based software package COCO [5, 6], which both use a collocation solver for the BVP and the pseudo-arclength continuation algorithms developed by Keller [21]. The idea for this setup is that each orbit segment is viewed as the solution to a vector field with time rescaled to the interval $[0, 1]$ and defined by boundary conditions at either end; the total integration time for each orbit segment is embedded as a problem parameter.

The method requires precise control of the phase of points on Γ, since we require knowledge of the phase ϑ_{o} at which the perturbation is applied, and the phase ϑ_{n} resulting from the perturbation. A key element of our method is to determine, via continuation, the point on Γ that has a particular phase, and conversely, to measure the phase of a particular point on Γ relative to the point $\gamma_0 \in \Gamma$ with phase zero. We measure ϑ_{n} via a pair of orbit segments that we call $\mathbf{g}$ and $\mathbf{w}$. Firstly, $\mathbf{g}$ is constrained as one complete cycle of Γ via the periodicity condition $\mathbf{g}(0) = \mathbf{g}(1)$ and total integration time $T_{\mathbf{g}} = T_\Gamma$. Consequently, the base point $\mathbf{g}(0)$, or equally $\mathbf{g}(1)$, is sure to lie in Γ. We then control the phase of $\mathbf{g}(0)$ with $\mathbf{w}$ by anchoring $\mathbf{g}(1)$ to the initial point $\mathbf{w}(0)$ of $\mathbf{w}$, and fixing $\mathbf{w}(1)$ to have zero phase. These conditions constrain $\mathbf{w}$ to lie on a portion of Γ for positive integration time $T_{\mathbf{w}}$. Since $\mathbf{w}(1)$ has zero phase, the phase of $\mathbf{w}(0)$ and, thus, $\mathbf{g}(0) = \mathbf{g}(1)$ is calculated from the integration time $T_{\mathbf{w}}$ of $\mathbf{w}$ as the fraction $\vartheta_{\mathrm{n}} = 1 - (T_{\mathbf{w}}/T_\Gamma)$. We control the phase ϑ_{o} that determines the point $\gamma_{\vartheta_{\mathrm{o}}} \in \Gamma$ at which the perturbation is applied by using the same mechanism. Hence, we define orbit segments $\mathbf{g}_{\mathbf{u}}$ and $\mathbf{w}_{\mathbf{u}}$ that play a similar role as $\mathbf{g}$ and $\mathbf{w}$, respectively; again, see [25] for full details.

We now describe how to compute the level curve of the isochron $I_{\vartheta_{\mathrm{n}}}$ that contains the point $(\vartheta_{\mathrm{o}}, A) = (\vartheta_{\mathrm{n}}, 0)$ on the periodic orbit Γ. To this end, we start a continuation run from the rotated solution $\mathbf{g} \equiv \Gamma$ with headpoint at phase ϑ_{n}, that is $\mathbf{g}(0) = \gamma_{\vartheta_{\mathrm{n}}}$. This continuation run solves for a family of orbit segments $\mathbf{u}$ with total integration time $T_{\mathbf{u}} = k\,T_\Gamma$ set to an integer k times the period of Γ. Each orbit segment $\mathbf{u}$ satisfies that its terminal point $\mathbf{u}(1)$ lies in the linear eigenspace $E(\gamma_{\vartheta_{\mathrm{n}}})$ of the isochron $I_{\vartheta_{\mathrm{n}}}$, at a (small) distance η from $\mathbf{g}(0) = \gamma_{\vartheta_{\mathrm{n}}}$. In other words, $\mathbf{u}$ satisfies the

two boundary conditions

$$\begin{aligned}[\mathbf{u}(1)-\mathbf{g}(0)]\cdot[\mathbf{u}(1)-\mathbf{g}(0)] &= \eta^2,\\ \mathbf{v}_{\vartheta_\mathrm{n}}^{\perp}\cdot[\mathbf{u}(1)-\mathbf{g}(0)] &= 0,\end{aligned}$$

where $\mathbf{v}_{\vartheta_\mathrm{n}}^{\perp}$ is the vector normal to the subspace $E(\gamma_{\vartheta_\mathrm{n}})$ at $\gamma_{\vartheta_\mathrm{n}}$. If η is sufficiently small, the phase of $\mathbf{u}(1)$ is well approximated by ϑ_n and, moreover, the initial point $\mathbf{u}(0)$ has the same phase ϑ_n, because $T_\mathbf{u}$ is an integer multiple of T_Γ.

The linearization of the isochron I_0 at γ_0, which is needed for the boundary conditions that define $\mathbf{w}$ and $\mathbf{w}_\mathbf{u}$, can be hard-wired in the problem, but ϑ_n may vary, in which case the normal vector $\mathbf{v}_{\vartheta_\mathrm{n}}^{\perp}$ must vary accordingly. We compute $\mathbf{v}_{\vartheta_\mathrm{n}}^{\perp}$ as the left eigenvector at $\gamma_{\vartheta_\mathrm{n}}$ associated with the trivial Floquet multiplier of Γ. Alongside the BVP that determines $\mathbf{g}$, the vector $\mathbf{v}_{\vartheta_\mathrm{n}}^{\perp}$ is given as the unit-length initial point of the periodic vector-bundle solution for the first variational equation

$$\dot{\mathbf{v}}_\mathbf{g} = -T_\mathbf{g}\,\mathrm{adj}[D_\mathbf{g}\mathbf{F}(\mathbf{g})]\,\mathbf{v}_\mathbf{g},$$

with boundary conditions

$$\begin{aligned}\mathbf{v}_\mathbf{g}(0)\cdot\mathbf{v}_\mathbf{g}(0) &= 1,\\ \mathbf{v}_\mathbf{g}(1)-\lambda\,\mathbf{v}_\mathbf{g}(0) &= 0,\end{aligned}$$

where $\lambda = 1$. Here, $\mathrm{adj}[D_\mathbf{g}\mathbf{F}(\mathbf{g})]$ is the adjoint of the Jacobian matrix of $\mathbf{F}$ evaluated over the periodic orbit $\mathbf{g}$; we refer to [25, 30] for details.

The primary level curve in the $(\vartheta_\mathrm{o}, A)$-plane is now defined by the curve of $(\vartheta_\mathrm{o}, A)$-pairs emanating from $(\vartheta_\mathrm{o}, 0)$ that correspond to the points $\mathbf{u}(0)$ in the family $\mathbf{u}$. Formally, we apply a phase reset from the point $\gamma_{\vartheta_\mathrm{o}} \in \Gamma$ in the direction $\mathbf{d}$ with amplitude A such that $\mathbf{u}(0) = \gamma_{\vartheta_\mathrm{o}} + A\,\mathbf{d}$, where we use the other rotated copy of Γ, given by the orbit segments $\mathbf{g}_\mathbf{u}$ and $\mathbf{w}_\mathbf{u}$, to define $\gamma_{\vartheta_\mathrm{o}}$ as the base point $\mathbf{g}_\mathbf{u}(0)$.

In total, the multi-segment BVP comprises the orbit segments $\mathbf{u}$, $\mathbf{g}$, $\mathbf{w}$, $\mathbf{g}_\mathbf{u}$, and $\mathbf{w}_\mathbf{u}$, as well as the vector bundle $\mathbf{v}_\mathbf{g}$ associated with $\mathbf{g}$. Hence, the dimension of the problem is $\mathrm{NDIM} = 6\,m$. The segments $\mathbf{g}$, with the bundle $\mathbf{v}_\mathbf{g}$, and $\mathbf{g}_\mathbf{u}$ have periodic boundary conditions, which gives $3\,m$ conditions together with the single normalization constraint for $\mathbf{v}_\mathbf{g}(0)$. The segments $\mathbf{w}$ and $\mathbf{w}_\mathbf{u}$ are anchored at $\mathbf{g}(1)$ and $\mathbf{g}_\mathbf{u}(1)$ and act as phase conditions, because their other end points pin the head points of $\mathbf{g}$ and $\mathbf{g}_\mathbf{u}$ to their required phases ϑ_n and ϑ_o, respectively; this gives another $2\,m$ conditions for $\mathbf{w}(0)$ and $\mathbf{w}_\mathbf{u}(0)$ and two conditions for $\mathbf{w}(1)$ and $\mathbf{w}_\mathbf{u}(1)$. Similarly, the segment $\mathbf{u}$ is pinned via the condition $\mathbf{u}(0) = \mathbf{g}_\mathbf{u}(0) + A\,\mathbf{d}$, adding another m boundary conditions, but we also require $\mathbf{u}(1) \in E(\gamma_{\vartheta_\mathrm{n}})$ sufficiently close to $\gamma_{\vartheta_\mathrm{n}}$, given by two additional boundary conditions. All these constraints add up to $\mathrm{NBC} = 6\,m + 5$ boundary conditions.

To find a one-dimensional level curve, we need $\mathrm{NPAR} = \mathrm{NDIM} - \mathrm{NBC} + 1 = 6$ free parameters. These parameters are the distance η, the integration times $T_\mathbf{g}$ and $T_{\mathbf{g}_\mathbf{u}}$, the Floquet multiplier λ, and two further parameters chosen from ϑ_o, A, and ϑ_n. Here, the integration times $T_\mathbf{w}$ and $T_{\mathbf{w}_\mathbf{u}}$ are defined as $T_\mathbf{w} = (\kappa - \vartheta_\mathrm{n})\,T_\Gamma$ (with $\kappa = 1$ or larger integer) and $T_{\mathbf{w}_\mathbf{u}} = (1 - \vartheta_\mathrm{o})\,T_\Gamma$, so while they may vary implicitly with ϑ_n or ϑ_o, they are not independent free parameters. On the other hand, the periods $T_\mathbf{g}$ and $T_{\mathbf{g}_\nu}$ and the trivial Floquet multiplier λ must remain free for a solution to exist, but their values do not vary significantly given the constraints of the problem.

We compute a primary level curve for the isochron with phase ϑ by starting the continuation run with a homotopy step from the known solution at $\vartheta_\mathrm{o} = \vartheta_\mathrm{n} = 0$ and $A = 0$; indeed, at $\vartheta_\mathrm{o} = \vartheta_\mathrm{n} = 0$ and $A = 0$, the solution is given by the orbit segments $\mathbf{g} = \mathbf{g}_\mathbf{u} = \Gamma$, $\mathbf{w} = \mathbf{w}_\mathbf{u} = \Gamma$, and $\mathbf{u}$ defined as k copies of Γ, with the parameter values $T_\mathbf{g} = T_{\mathbf{g}_\mathbf{u}} = T_\Gamma$, $\lambda = 1$, and $\eta = 0$; here

$\mathbf{v_g}$ is given by the vector bundle starting at γ_0, which is either known or computed separately as described in [25, 30]. In the homotopy step, we shift the phase of the periodic components such that their base points lie at $\gamma_\vartheta \in \Gamma$. During this step, we increase ϑ_o up to $\vartheta_\mathrm{o} = \vartheta$ and ϑ_n is free. The parameter $A = 0$ remains fixed, so that the solution family requires $\vartheta_\mathrm{n} = \vartheta_\mathrm{o}$ during this step. As soon as $\vartheta_\mathrm{n} = \vartheta$, we are ready to compute the primary level curve in L_ϑ by continuation: in this step, we fix $\vartheta_\mathrm{n} = \vartheta$ while ϑ_o and A are free, so they take on the appropriate phase-amplitude coordinates along the primary level curve; other components in the level set L_ϑ must be found by additional homotopy steps; for example, by fixing A and varying ϑ_o and ϑ_n, so that level curves separating two components can be crossed.

Illustration of the method for a planar example

We illustrate our method with a planar example to highlight the essence of computing a level curve of the phase-resetting surface in the $(\vartheta_\mathrm{o}, A)$-plane, instead of the one-dimensional isochron in the phase plane (which would be a one-dimensional slice of an isochron in case of a higher-dimensional system). Recall that the phase-resetting surface $\mathrm{graph}(\mathcal{P}_\mathbf{d})$ is a function over the $(\vartheta_\mathrm{o}, A)$-plane, which means that each point $(\vartheta_\mathrm{o}, A)$ is associated with a unique value for $\vartheta_\mathrm{n} \in [0, 1)$. Hence, if we compute a level curve for fixed ϑ_n then the initial point $\mathbf{u}(0)$ of the orbit segment $\mathbf{u}$ in the associated solution family traces out a curve on the isochron I_{ϑ_n} in state space. It is important to realize that, even in the case of a planar system, $\mathbf{u}(0)$ does not typically trace out the entire isochron I_{ϑ_n}, while the continuation does give the complete level curve in the $(\vartheta_\mathrm{o}, A)$-plane (up to a finite arclength); indeed, the range of the perturbation map $\Upsilon_\mathbf{d}$ is only the half-cylinder $\mathcal{C}_\mathbf{d}$ rather than the full state space.

Specifically, we consider the planar system (11) from Section 4.1, where we considered the phase-resetting surface of the attracting periodic orbit Γ for the direction $\mathbf{d} = (1, 0)^\mathrm{T}$, parallel to the x-axis. Figure 11 illustrates the first part of computing the primary level curve in $L_{0.15}$ associated with $I_{0.15}$ as A increases from $(\vartheta_\mathrm{o}, A) = (0.15, 0)$. Panel (a) shows this computed curve, labeled $L_{0.15}$ (blue), in the $(\vartheta_\mathrm{o}, A)$-plane; the point $\gamma_{0.15} \in \Gamma$ at $A = 0$ is labeled, as are four other points on this level curve that correspond to particular events during the computation; panels (b), (c) and (d) depict the representation in the (x, y)-plane for the points labeled p_b, p_c and p_d, respectively. In each of these panels, we show, in black, the attracting periodic orbit Γ together with the zero-phase point γ_0, and the attracting equilibrium $\mathbf{x}_s$ inside the unstable periodic orbit Γ_u that forms the basin boundary of Γ. Furthermore, we plot the portion of $L_{0.15}$ (blue) up to the initial point on the orbit segment $\mathbf{u}$ (green curve) that corresponds to the labeled point in panel (a); hence, $\mathbf{u}$ is the response after the perturbation $\Upsilon_\mathbf{d}(\vartheta_\mathrm{o}, A) = \gamma_{\vartheta_\mathrm{o}} + A\,\mathbf{d}$ (dashed line) for the $(\vartheta_\mathrm{o}, A)$-coordinates of the labeled point in panel (a). For illustrative purposes, we set the integration time for $\mathbf{u}$ to only a single period of Γ (that is, $k = 1$). Note that $\mathbf{u}$ ends in the linearization of $I_{0.15}$ at the labeled point $\gamma_{0.15}$ as suggested by the straight line (turquoise) that represents $\mathbf{v}_{0.15}$ and extends the plotted part of $I_{0.15}$, and the perpendicular straight line (orange) that represents $\mathbf{v}^\perp_{0.15}$.

The continuation starts from $A = 0$ with $\vartheta_\mathrm{o} = \vartheta_\mathrm{n} = 0.15$ in panel (a), so that $\mathbf{u}(0) = \gamma_{0.15}$. As A increases, $\mathbf{u}(0)$ is forced away from Γ and, since ϑ_n is fixed, it must trace the one-dimensional isochron $I_{0.15}$. Consequently, the orbit segment $\mathbf{g_u}$ that determines the value for ϑ_o shifts around Γ in order to maintain the condition $\mathbf{u}(0) = \mathbf{g_u}(0) + A\,\mathbf{d} = \gamma_{\vartheta_\mathrm{o}} + A\,\mathbf{d}$. Hence, as A increases from 0, the point $\gamma_{\vartheta_\mathrm{o}}$ at which the perturbation is applied moves down along Γ, away from γ_0, which means that ϑ_o increases as well. Note that the initial point $\mathbf{u}(0)$ cannot move outside the (collapsed) cylinder $\mathcal{C}_\mathbf{d}$, that is, into the dark-gray shaded regions in panels (b)–(d). Therefore, $\mathbf{u}(0)$ can only trace the 'outgoing' branch of $I_{0.15}$ until $\mathbf{g_u}(0)$ reaches a minimum with respect to the y-coordinate at the point $\gamma_{0.25} = (0, -1)$ on Γ. This is the situation depicted in panel (b),

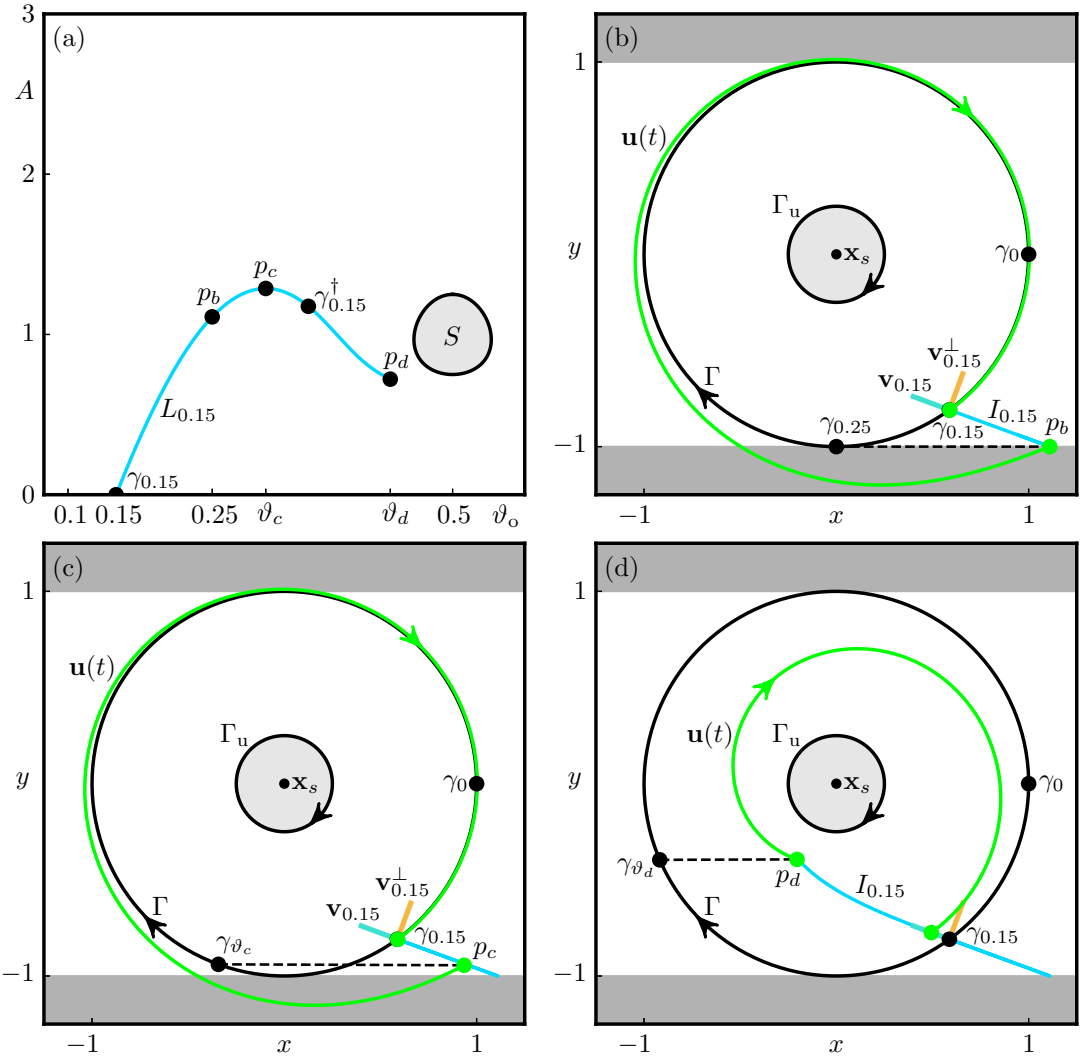

Figure 11: Computing the primary level curve, labeled $L_{0.15}$ (blue), of $I_{0.15}$ for the planar system (11) in the direction $\mathbf{d} = (1, 0)^{\mathrm{T}}$. Panel (a) shows $L_{0.15}$ in the (ϑ_o, A)-plane, with the points p_b, p_c and p_d marking the (ϑ_o, A)-pairs that correspond to the setup in state space illustrated in panels (b), (c) and (d), respectively. Here, we show Γ, Γ_u (black curves) and $\mathbf{x}_s$ (black point) together with the points γ_0 and $\gamma_{0.15}$ with two straight-line segments indicating the perpendicular vector $\mathbf{v}^\perp_{0.15}$ (orange) and the linearization of $I_{0.15}$ (turquoise); also shown is the isochron $I_{0.15}$ (blue curve) up to the initial point on the orbit segment $\mathbf{u}$ (green curve) that results from the perturbation at phase ϑ_o of amplitude A (dashed line) for the correspondingly labeled point in panel (a).

where $\mathbf{u}(0) \approx (1.1098, -1.0)$ is given the same label p_b as the point $(\vartheta_o, A) \approx (0.25, 1.1098)$ in panel (a). While there is nothing significant about the point labeled p_b in panel (a), the corresponding point p_b in panel (b) is special: as the continuation proceeds, both A and ϑ_o increase further, with γ_{ϑ_o} now moving up along the left side of Γ, so that $\mathbf{u}(0)$ changes direction and starts to retrace the previously computed portion of $I_{0.15}$. Indeed, since Γ is planar, there are two (ϑ_o, A) pairs that define a point $\gamma_\vartheta \in \Gamma$, for all $\vartheta \in (-0.25, 0.25)$ (modulo 1). The primary level curve in $L_{0.15}$ attains a maximum in A at the point $(\vartheta_o, A) \approx (0.3057, 1.2869)$ labeled p_c in panel (a). In the corresponding panel (c), one can, perhaps, appreciate that the perturbation amplitude is maximal from the point labeled γ_{ϑ_c}, but the point labeled p_c on $I_{0.15}$ is not otherwise special. Note that, as the continuation progresses further, $\mathbf{u}(0)$ reaches $\gamma_{0.15}$ again, exactly when

$\vartheta_o = 0.25 + (0.25 - 0.15) = 0.35$ and $A = 2\cos(0.15 \times 2\pi) \approx 1.1756$, which occurs at the point labeled $\gamma^{\dagger}_{0.15}$ in panel (a). The continuation ends at the point labeled p_d in panel (a), when η has reached the (admittedly rather large) tolerance $\eta = \eta_{\max} = 0.1$. For the computation of the level curves in Fig. 4, we used $\eta_{\max} = 10^{-4}$ and $k = 10$ times the period of Γ for the integration time $T_{\mathbf{u}}$ of the orbit segment $\mathbf{u}$.

References

[1] Arnold VI. *Singularity Theory*, Cambridge: Cambridge University Press; 2013.

[2] Best EN. Null space in the Hodgkin–Huxley equations. A critical test. *Biophys J*, **27**(1): 87–104, 1979.

[3] Brown E, Moehlis J, Holmes P. On the phase reduction and response dynamics of neural oscillator populations, *Neural Comput*, **16**(4): 673–715, 2004.

[4] Chay TR, Lee YS. Phase resetting and bifurcation in the ventricular myocardium. *Biophys J*, **47**(5): 641–651, 1985.

[5] Dankowicz H, Schilder F. Continuation Core and Toolboxes (COCO): Toolboxes for parameter continuation and bifurcation analysis; 2009. available from http:www.sourceforge.net/projects/cocotools/

[6] Dankowicz H, Schilder F. *Recipes for Continuation* Philadelphia: SIAM Publishing; 2013

[7] Demazure M. *Bifurcations and Catastrophes: Geometry of Solutions to Nonlinear Problems*, Berlin, Heidelberg: Springer-Verlag; 2000.

[8] Doedel EJ. AUTO: A program for the automatic bifurcation analysis of autonomous systems. *Congressus Numerantium* **30**: 265–284, 1981.

[9] Doedel EJ, Oldeman BE. AUTO-07P: Continuation and bifurcation software for ordinary differential equations. With major contributions from Champneys AR, Dercole F, Fairgriev TF, Kuznetsov YuA, Paffenroth RC, Sandstede B, Wang XJ, Zhang CH, 2007. Available from http://cmvl.cs.concordia.ca/auto

[10] Ermentrout GB. Type I membranes, phase resetting curves, and synchrony. *Neural Comput*, **8**(5): 979–1001, 1996.

[11] Ermentrout GB, Terman DH. *Mathematical Foundations of Neuroscience*. Interdisciplinary Applied Mathematics **35**, New York: Springer-Verlag; 2010.

[12] Ermentrout GB, Glass L, Oldeman BE. The shape of phase-resetting curves in oscillators with a saddle node on an invariant circle bifurcation. *Neural Comput*, **24**(12): 3111–3125, 2012.

[13] FitzHugh R. Impulses and physiological states in theoretical models of nerve membrane. *Biophys J* **1**(6): 445–466, 1961.

[14] Glass L, Winfree AT. Discontinuities in phase-resetting experiments, *Am J Physiol Regul Integr Comp Physiol*, **246**(2): R251–R258, 1984.

[15] Guckenheimer J. Isochrons and phaseless sets. *J Math Biology*, **1**: 259–273, 1975.

[16] Hannam J, Krauskopf B, Osinga HM. Global manifolds of saddle periodic orbits parametrised by isochrons. In: Olaru S, Elaydi S, Cushing J, Lozi R, editors. *Advances in Discrete Dynamical Systems, Difference Equations, and Applications* (ICDEA 2022). Springer Proceedings in Mathematics & Statistics, Vol. 444. Berlin: Springer-Verlag; 2024, pp 143–174.

[17] Hannam J, Krauskopf B, Osinga HM. Isochron foliations and global bifurcations: a case study. *Trans Math Appl*, **6**(2): tnac002, 2022.

[18] Hansel D, Mato G, Meunier C. Synchrony in excitatory neural networks, *Neural Comput*, **7**(2): 307–337, 1995.

[19] Hodgkin AL. The local electric changes associated with repetitive action in a non-modulated axon, *J Physiol*, **107**(2): 165–181, 1948.

[20] Hodgkin AL, Huxley AF. A quantitative description of membrane current and its application to conduction and excitation in nerve. *J Physiol*, **117**(4): 500–544, 1952.

[21] Keller HB. *Lectures on Numerical Methods In Bifurcation Problems*. Tata Institute Of Fundamental Research. Heidelberg: Springer-Verlag; 1986.

[22] Krauskopf B, Osinga HM, Galán-Vioque J. *Numerical Continuation Methods for Dynamical Systems*. Understanding Complex Systems, Berlin: Springer-Verlag; 2007.

[23] Langfield P, Krauskopf B, Osinga HM. Solving Winfree's puzzle: the isochrons in the Fitzhugh–Nagumo model. *Chaos*, **24**(1): 013131, 2014.

[24] Langfield P, Krauskopf B, Osinga HM. Forward-time and backward-time isochrons and their interactions. *SIAM J Appl Dynam Syst*, **14**(3): 1418–1453, 2015.

[25] Langfield P, Krauskopf B, Osinga HM. A continuation approach to computing phase resetting curves. In: Junge O, Schütze O, Froyland G, Ober-Blobaum S, Padberg-Gehle K, editors. *Advances in Dynamics, Optimization and Computation. SON 2020*, Studies in Systems, Decision and Control, Vol. 304, Berlin: Springer-Verlag; 2020, pp 3–30.

[26] Lee KH, Broderick NGR, Krauskopf B, Osinga HM. Generic planar phase resetting near a phaseless point. *ANZIAM J*, in press.

[27] Lee KH, Broderick NGR, Krauskopf B, Osinga HM. Phase response to arbitrary perturbations: Geometric insights and resetting surfaces. *Discrete & Continuous Dynamical Systems — Series B*, 2024, Online First.

[28] Mauroy A, Mezić I. On the use of Fourier averages to compute the global isochrons of (quasi) periodic dynamics. *Chaos*, **22**(3): 033112, 2012.

[29] Nagumo J, Arimoto and S. Yoshizawa S. An active pulse transmission line simulating nerve axon. *Proc IRE* **50**(10): 2061–2070, 1962.

[30] Osinga HM, Moehlis J. Continuation-based computation of global isochrons. *SIAM J Appl Dynam Syst*, **9**(4): 1201–1228, 2010.

[31] Pérez-Cervera A, Seara TM, Huguet G. Global phase-amplitude description of oscillatory dynamics via the parameterization method. *Chaos*,**30**(8): 083117, 2020.

[32] Poston T, Stewart IN. *Catastrophe Theory and its Applications*, Mineola, NY: Dover Publications; 1996.

[33] Shilnikov AL, Porter Maurer A. The art of grid fields: geometry of neuronal time. *Front Neur Circ*, **10**: 12, 2016.

[34] Winfree AT. Time and timelessness in biological clocks. In: Urquhart J, Yates FE, editors. *Temporal Aspects of Therapeutics*, ALZA Conference Series Vol. **2** Berlin: Springer-Verlag; 1973, pp 35–49.

[35] Winfree AT. Patterns of phase compromise in biological cycles. *J Math Biology*, **1**(1): 73–93, 1974.

[36] Winfree AT. *The Geometry of Biological Time*, 2nd ed., New York: Springer-Verlag; 2001.

[37] Winfree AT. Sudden cardiac death: a problem in topology. *Sci American*, **248**(5): 144–161, 1983.